The sedimentary flux of dissolved rare earth elements to the ocean

April N. Abbott[1], Brian A. Haley[1], James McManus[1, 2], Clare E. Reimers[1]

[1]College of Earth, Ocean, and Atmospheric Sciences, Oregon State University, 104 CEOAS Admin. Bldg., Corvallis, OR 97331-5503

[2]University of Akron, Department of Geoscience, Akron, OH 44325-4101

Abstract

We determined pore fluid rare earth element (REE) concentrations in near-surface sediments retrieved from the continental margin off Oregon and California (USA). These sites represent shelf-to-slope settings, which lie above, within, and below the oxygen minimum zone of the Northeast Pacific. The sediments are characterized by varying degrees of net iron reduction, with pore waters from the shelf sites being generally ferruginous, and the slope sediments having less-pronounced iron reduction zones that originate deeper in the sediment package. REE concentrations show maxima in shallow (upper 2-10 cm) subsurface pore fluids across all sites with concentrations that rise more than two orders of magnitude higher than seawater. These pore fluid enrichments highlight the importance of a sedimentary source of REEs to the ocean's water column. Here we use our measurements to estimate the diffusive flux of Nd out of ocean sediments resulting in a global flux between 18 and 110 x 10^6 mol Nd yr^{-1}. While we do assume that our pore fluid profiles as well as the very limited data previously published are representation of a wide array of ocean environments, this calculated flux can account for the modeled missing Nd source flux (76 x 10^6 mol Nd yr^{-1}) in global budgets (Arsouze et al., 2009). Pore fluid normalized REE patterns show distinct variation in the middle REE and heavy REE enrichments with sediment depth and amongst sites. These patterns show that the heavy REE enrichment of pore fluids at our deep slope site (3000 m water depth) is closest to the heavy REE enrichment of seawater. This observation supports the view that REE cycling within the upper ten centimeters of deep-sea marine sediments, as opposed to shallower continental shelf and slope sediments, plays a significant role in controlling the integrated global REE flux from the pore fluids and

consequently the broad-scale REE pattern in seawater.

Keywords: Rare Earth Elements, pore fluid, neodymium, benthic flux

1. Introduction

The lanthanides, also referred to as the rare earth elements (REEs), are a series of elements that exist dominantly in a trivalent state in the environment, with the exceptions of Eu and Ce, which can exist as Eu (II) and Ce (IV) (Elderfield and Greaves, 1982). In the ocean, the REEs are generally depleted in surface waters and show increasing enrichment with depth (Elderfield, 1988; Bertram and Elderfield, 1993; Goldstein and Hemming, 2003; Lacan et al., 2012). Additionally, the REEs are typically found in higher concentrations in the deep Pacific relative to the deep Atlantic Ocean (e.g., Goldstein and Hemming, 2003). These observations suggest that particle scavenging within the upper water column and particle dissolution and exchange at depth control the oceanic distribution of the REEs (Elderfield, 1988; Bertram and Elderfield, 1993; Sholkovitz et al., 1994). In addition to these general trends for the REEs, specific trends for Ce are observed because of the anomalous behavior of Ce (IV) (e.g. Moffet, 1990). A Ce anomaly reflects microbially mediated oxidation followed by preferential scavenging of Ce (IV) in seawater (Moffet, 1990). The Ce anomaly is defined as the difference ratio of the predicted Ce based on neighboring REEs to the measured Ce (e.g. Elderfield 1988; Byrne and Sholkovitz, 1996; Grenier et al., 2013; Pearce et al., 2013). As such, the Ce anomaly is dependent on the behavior and concentrations of neighboring trivalent REEs and must be interpreted with caution (Elderfield and Pagett, 1986; De Baar et al., 1988; Sholkovitz et al., 1989; Bau and Dulski, 1996; Alibo and Nozaki, 1999; Tachikawa et al., 1999; Haley et al., 2004; Kim et al., 2012).

Individual REEs and the REEs as a series are powerful geochemical tracers because of their predictable behavior and they have been used in oceanographic studies

71 highlighting redox conditions (e.g., Liu et al., 1988; Sholkovitz and Schneider, 1991),
72 particulate exchange and scavenging processes (e.g Andersson et al., 2008; Oka et al.,
73 2009), and water mass transport (e.g. Scher and Martin, 2004; Andersson et al., 2008;
74 Haley et al., 2008). While these and many other efforts (e.g. Goldberg et al., 1963;
75 Palmer and Elderfield, 1986; Sholkovitz, 1990, 1992; German et al., 1995; Sherrell et al.,
76 1999; Schijf and Byrne, 2004; Schacht et al., 2010; Johannesson et al., 2011; Haley et al.,
77 2013) have greatly expanded our knowledge of marine REEs, our understanding of the
78 sources of REEs to seawater as well as the processes that define the seawater REE
79 signature is incomplete. Although the riverine flux is, at present, thought to be the
80 primary input of REEs to the oceans (e.g. Martin et al., 1976; Greaves et al., 1994;
81 Sholkovitz et al., 1999) attempts to balance the budget of the REEs have not been entirely
82 successful (e.g. Keasler and Loveland 1982; Bertram and Elderfield, 1993; van de Flierdt
83 et al., 2004). Recent work has proposed submarine groundwater discharge as a potentially
84 significant source for Nd in the accounting of REE fluxes to the oceans (Johannesson and
85 Burdige, 2007; Johannesson et al., 2011). Similarly, the flux of REEs from marine pore
86 fluids has been suggested to be a significant source of marine REEs, with calculated pore
87 fluid exchange rates being higher than the combined total of all other marine source
88 fluxes (Elderfield and Sholkovitz, 1987; Sholkovitz et al., 1989; Sholkovitz, 1992; Haley
89 et al., 2003; Arsouze et al., 2009). Because of these and other outstanding questions
90 regarding the marine REE cycle, there are significant limitations with respect to the
91 utility of REEs in oceanographic studies.
92 Understanding how the REEs fractionate from one another under various natural
93 conditions can supply additional information that will allow us to address a number of

94 these outstanding questions regarding global REE cycles. Fractionation among the REEs
95 is observed by examining the REE "patterns", which are the REE concentrations
96 normalized to shale values. This normalization facilitates inter-REE comparisons despite
97 large variations in natural abundances. These REE patterns are tools for diagnosing the
98 potential processes that control the distribution and fractionation of REEs (e.g.
99 Sholkovitz et al., 1999; Haley et al., 2004). Fractionation across the series of REEs
100 occurs because of the systematic decrease in ionic radius with increasing atomic number
101 due to the progressive filling of inner f-shell electrons. This fractionation suggests that
102 the budget for each REE may be somewhat different. Particulate-water interactions,
103 dissimilar source and sink terms, complexation, oxide scavenging, and REE
104 incorporation into solid phases can each contribute to changes in the ocean's REE pattern
105 (Cantrell and Byrne, 1987; Lee and Byrne, 1993; Schijf and Byrne, 2004; Leybourne and
106 Johannesson, 2008; Akagi, 2013). The resulting fractionation varies as a result of,
107 among other factors, the nature of the complexing agent (e.g. inorganic and organic
108 ligands, carbonate, oxalate, silicic acid), the presence of sulfates or phosphates, pH, and
109 ionic strength (e.g. Cantrell and Byrne, 1987; Schijf and Byrne, 2004; Tang and
110 Johannesson, 2010; Akagi, 2013). Each of the above processes, including complexation
111 and oxide scavenging, may have a unique characteristic fractionation. The ability to
112 associate a specific pattern with a factor (e.g. pH, complexation agent) or a process (e.g.
113 complexation, oxide scavenging) facilitates interpretations of pattern changes and
114 controls on the REE budget (e.g. Sholkovitz et al., 1994; Akagi, 2013).
115 Processes causing REE fractionation determine the oceanic REE pattern, which is
116 clearly altered from the pattern of various potential sources of REE including the riverine

117 source (e.g. Elderfield et al., 1990; Sholkovitz et al., 1999; Leybourne and Johannesson,
118 2008, Stolpe et al., 2013) and the pattern of riverine suspended particles (Sholkovitz et
119 al., 1999, Censi et al., 2007, Stolpe et al., 2013). When normalized to shale, seawater is
120 characterized by a heavy REE (HREE, including Er, Tm, Yb, and Lu) enriched pattern
121 with a pronounced negative Ce anomaly (Goldberg et al., 1963; Högdahl et al., 1968;
122 Elderfield and Greaves, 1982; Klinkhammer et al., 1983; Elderfield, 1988; Piepgras and
123 Jacobsen, 1992). In contrast to the HREE enriched pattern typical of seawater, dissolved
124 riverine REE patterns are typically MREE enriched (e.g. Sholkovitz et al., 1999, Stolpe et
125 al., 2013). Additionally, suspended riverine and estuarine particulates have a flat (shale-
126 like) REE pattern or a MREE enriched pattern (e.g. Sholkovitz et al., 1999; Sholkovitz
127 and Szymczak, 2000; Censi et al., 2007, Stolpe et al., 2013). Similar HREE depletions
128 have also been reported in bottom sediments from estuarine settings (e.g. Censi et al.,
129 2007) and riverbeds (Sholkovitz, 1999). These HREE depletions have been attributed to
130 the preferential settling of larger grain sizes that carry HREE enriched heavy minerals
131 (Sholkovitz et al., 1999). Fractionation of the REEs certainly influences these elements
132 during transport, but there is still a fundamental discrepancy between the REE patterns of
133 REE sources to the ocean and the REE pattern of seawater. This discrepancy between the
134 oceanographic REE signature and that of the sources is at the heart of our knowledge gap
135 in REE geochemistry.
136 Given the importance of a benthic source to the ocean's REE balance, the REE
137 patterns in pore fluid will be important for constraining the significance of particle-fluid
138 interactions for controlling REEs. Pore fluid REE patterns are a function of the
139 competition between REEs being introduced into the fluid phase (from a sedimentary

source) and the REEs being removed from solution (Haley et al., 2004). REE sources and sinks may act preferentially on specific REEs and result in fractionation. Precipitation of phosphate bearing minerals (e.g. Koeppenkastrop and De Carlo, 1993; Kuss et al. 2001), degradation of organic material, organic matter coatings (Byrne and Kim, 1990), weathering of REE rich phosphates (e.g. Censi et al. 2007), and volcanic ash (Schacht et al., 2010) have all been shown to exert influence over pore fluid REE distributions and these processes can each have specific REE signatures. Existing data from pore fluids show that REE patterns fit into one of three general categories (Elderfield and Sholkovitz 1987; Sholkovitz et al., 1989; Haley et al., 2004; Schacht et al., 2010; Kim et al., 2012): (1) those with a constant ("linear") but moderate increase in PAAS-normalized REEs across the series from light to heavy, (2) those having a middle REE (MREE, including Eu, Gd, Tb, and Dy) enrichment or "bulge," or (3) those with a marked HREE enrichment – much like seawater (Haley et al., 2004). REE patterns in anoxic pore fluids tend to be characterized by a MREE "bulge" pattern in the ferruginous zone (Haley et al., 2004; Kim et al., 2012). Deeper anoxic pore fluids within the sulfidic and methanogenic zones have linear REE patterns or are HREE enriched (Kim et al., 2012). The HREE enriched pattern is consistent with preferential complexation of HREEs after REE release from organic matter degradation (Goldberg et al., 1963; Byrne and Sholkovitz, 1996; Haley et al., 2004). The REE pattern observed in pore fluid is a result of the combined source and sink terms acting on these fluids. Therefore, the pore fluid REE pattern can be used to identify the mechanistic influences on pore fluid REE geochemistry if the fractionation caused by the source or sink is known.

Identifying the mechanistic influences on pore fluid REE patterns has been limited by the scarcity of pore fluid REE data. Understanding these mechanisms is essential to constraining the fluid-particle interactions that would generate a marine sedimentary REE source. Here, we present pore fluid REE profiles collected from eight sites across the continental margin of Oregon and California (USA). Our sites are continental margin environments with site locations above, within, and below the eastern North Pacific's oxygen minimum zone. These sites provide additional data to constrain how diagenesis influences REE distributions and allow us to estimate the flux of dissolved REEs to the ocean from marine sediments.

2. Study Sites and methods

2.1 Study Sites

Pore fluid was collected from eight sites in the eastern North Pacific along the Oregon and California margin (**Figure 1, Appendix Table 1**). Samples were collected over the course of three cruises: in September 2007 (Stations 1, 2, 3, and 6), October 2012 (HH500, HH1200, and HH3000), and July 2013 (HH200, same location as Station 2). The sites off the Oregon margin are divided into shelf sites (Station 1, open diamond; Station 2, open triangle; and HH200, closed triangle) and slope sites (HH500, closed diamond; HH1200, closed circle; and HH3000, closed square). Together these six sites form a shallow (105 m) to deep (3060 m) east-west transect near the mouth of the Umpqua River (Oregon). Despite the general proximity to the Umpqua River, the shelf sites do not represent the river's depositional center as this locality is well defined by previous work and is south of our sites as indicated by reactive iron and manganese contents, δC_{org}, C:N, and ligand measurements (Hastings et al., 2012; Roy et al., 2013);

185 therefore, these sites are representative of the more general continental shelf setting along
186 this margin (e.g., Hastings et al., 2012; McManus et al., 2012; Roy et al., 2013), which is
187 influenced by both autochthonous and riverine inputs. Both California margin sites
188 (Station 3, open circle and Station 6, open square **Figure 1**) are shelf sites (water depths
189 ~100 m), adjacent to the mouth of the Eel River (California). Closed symbols indicate
190 sites visited in October 2012 and July 2013, open symbols are those sites visited in
191 September 2007 that had adequate sample volumes for REE analyses (McManus et al.,
192 2012).

193 The sediments of the Oregon-California margin generally have a large terrestrial
194 influence and are characterized by relatively high C_{org} (1 to 2 wt %) and relatively low
195 $CaCO_3$ (<0.5%) (Lyle et al., 2000; Roy et al., 2013; Hastings et al., 2012). Sedimentation
196 is seasonally variable, with the annual period of high sediment deposition typically
197 falling from October to March (Kniskern et al., 2011). The Eel River and the Umpqua
198 River have many contrasting geologic and discharge characteristics. There is an order-
199 of-magnitude greater sediment discharge from the Eel River compared to the Umpqua
200 (~18×10^9 kg versus ~1.4×10^9 kg, respectively; Wheatcroft and Sommerfield, 2005) and
201 higher sedimentation rates near the Eel River sites compared to near the Umpqua River
202 slope sites. Previous studies from the Oregon-California margin indicate sedimentation
203 rates between 0.2-1.4 cm yr^{-1} on the shallow shelf near the Eel River (Sommerfield and
204 Nittrouer, 1999) and sedimentation rates between 1.1 to 2.4 mm yr^{-1} at our Umpqua River
205 shelf sites (Station 1 and Station 2, HH200; McManus et al., 2012; also see Wheatcroft et
206 al., 2013). Additionally, high discharge events are less frequent in the Umpqua River
207 than the Eel River (Goñi et al., 2013). The Eel drainage basin consists largely of marine

208 sedimentary rocks (sandstones and shales) in contrast to the Umpqua drainage basin,
209 which consists of the sedimentary Tyee Formation (siltstones, sandstones) and volcanics
210 (http://www.nationalatlas.gov/; Kniskern et al., 2011 and sources therein). The Umpqua
211 River's suspended particulate organic matter is dominated by biogenic sources compared
212 to the Eel River which has significant petrogenic derived organic matter, which is highly
213 diluted by suspended mineral particulates (Goñi et al., 2013). In the shallower reaches of
214 the continental margin, sand content can be quite high (Kulm et al., 1975) with content
215 up to 40% documented on the shallow (~100 m) shelf near the Umpqua and
216 amounts of sand decreasing off shore (<20% by 200 m water depth, Kulm et al.,
217 1975). In the same study, the amount of clay was shown to increase from less than
218 20% in 100 m water depth to up to 40% by 200 m (Kulm et al., 1975). In terms of
219 clay mineral abundances, the Umpqua and nearby rivers have higher smectite/illite
220 ratios (2.3-3.1) than the Eel river (0.3 - 0.8; VanLaningham et al., 2008).

221 The Northeast Pacific oxygen minimum zone occurs between the depths of 600
222 and 900 m along the Oregon shelf (**Figure 2a**). Bottom depth for each coring site is
223 indicated on the water column oxygen profile from site HH3000 (**Figure 2**). Slope sites
224 (HH500, HH1200, and HH3000) are located below the water column thermocline
225 (**Figure 2b**) and halocline (**Figure 2c**). The dissolved oxygen, temperature, and salinity
226 profiles observed at all the Oregon transit sites would be indistinguishable from each
227 other if overlain on the scale of Figure 2.

228 **2.2 Sampling and Pore fluid extraction**

229 Unfiltered and filtered water column samples were collected from 12 depths at
230 HH1200 and HH3000 and five depths at HH500 (**Appendix table 2**). For unfiltered

231 samples, seawater was collected directly from the Standard PVC Niskin bottle into an
232 acid cleaned cubitainer. Niskin bottles were not cleaned prior to deployment. For
233 filtered samples, the Niskin bottles were pressurized using N_2, which facilitated filtration
234 of seawater using in-line "Disposal A" 0.45 μm filters with a white acrylic copolymer
235 coating over a non-woven substrate (Geotech Environmental item 73050004) during
236 direct transfer into acid cleaned cubitainers. All samples were acidified to pH ≤2.5 using
237 12 M HCl.

238 Sediment cores were collected using a multi-corer (Barnett et al., 1994). Pore
239 fluid samples were extracted only from cores that appeared on visual inspection to be
240 intact and of similar integrity. Clarity of the water at the interface, the lack of slope of the
241 sediment surface, core seal, and gaps in the sediment along the core liner were used as
242 visual guides to evaluate core integrity following recovery. Additionally, cores with
243 macrofauna present (e.g. sea urchins) were generally excluded, although on occasion we
244 encountered these organisms during core processing and they were discarded. The
245 selected cores were sectioned in an anoxic glove bag, and sediment intervals transferred
246 into 85 mL centrifuge tubes, and centrifuged at 10,000 – 12,000 rpm for 15 minutes.
247 Pore fluid was syphoned off the top of each tube in a second anoxic glove bag and
248 filtered using PALL ® acrodisc syringe filters with a 0.45μm Supor ® membrane. When
249 processing samples from the HH200, HH500, HH1200, and HH3000 sites, corresponding
250 intervals from multiple cores were combined after filtering to create large volume pore
251 fluid samples (for isotope analyses not reported here). These samples were acidified to
252 pH ~2 and kept refrigerated until analysis. Samples from HH200, HH500, HH1200, and
253 HH3000 were typically analyzed within a month of collection. Smaller volume

individual core samples were collected from Stations 1, 2, 3 and 6 using the same centrifuge technique (Severmann et al., 2010), and were analyzed in 2012. We also collected samples for REE concentration measurements using Rhizon pore fluid sampling devices; however, we found that these samplers remove more than half of HREEs from solution during collection and can introduce a substantial LREE blank (see **Appendix A.2**) and cannot be used for REE determinations.

2.3 Analytical Methods

2.3.1 REE separation

The rare earth elements were separated from 10 mL samples of the pore fluid or seawater using a column with 2 mL of BioRad Analytical Grade Chelex ® 100 resin (100-200 mesh, sodium form CAT#142-2832). These columns were optimized for REE yield (>80% with calibration standards) and effective Ba removal. Before separations, the resin was cleaned with 10 mL of 3M HNO_3 and conditioned with 10 mL of chelation concentration reagent 2.0 M ammonium acetate (pH 5.4 ± 0.1, Dionex or Thermo Scientific). For samples that did not have 10 mL available, the maximum volume available was loaded onto the column. Each sample was buffered with 100 µL of the 2.0 M ammonium acetate immediately prior to column loading to bring the sample from pH 2 to pH 5. Following the sample addition, 15 mL of 2.0 M ammonium acetate was eluted prior to collecting the REEs in 12 mL of 3 M HNO_3 (final pH 1 to 2). Calibration standards, including blanks, made using a known amount of REE in 10 mL of a NaCl (0.6 M) and Ba (95 µM) solution, were also run through the columns. The resulting solutions were used for the standard curve on the ICP-MS. The consistency of our standard curve was verified by seawater sample NBP95R10, which has greater Ba

277 concentrations, and therefore greater Ba oxide interference potential than our pore fluid
278 samples. The REE fraction was analyzed using a Thermo VG ExCell quadropole ICP-MS
279 at the W.M. Keck Laboratory for Plasma Mass Spectrometry (Oregon State University).
280 The ICP-MS was tuned to minimize oxide formation (<3%) in the plasma stream. The
281 isotopes monitored as well as the ICP-MS running parameters are given in **Appendix**
282 **Table 8**. A seawater sample (NBP95R10) collected from the Bransfield Strait in the
283 Southern Ocean (62° 46'S, 59° 24'W, 1300 m water depth) was used as an in-house
284 consistency standard (no calibrated seawater or pore fluid REE standards are available).
285 This chromatography technique is accurate to ± 1σ values ranging from 0.2 to 4 pM for
286 REEs in NBP95R10 (**Appendix Table 2**). The limit of detection (**Appendix Table 3**)
287 was below the procedural blank (4.2 pM La, 6.8 pM Ce, 0.8 pM Pr, 3.5 pM Nd, 0.5 pM
288 Sm, 0.7 pM Eu, 0.3 pM Gd, 0.1 pM Tb, 0.3 pM Dy, 0.1 pM Ho, 0.2 pM Er, 0.05 pM Tm,
289 0.1 pM Yb, and 0.3 pM Lu) for all REEs. However, pore fluid samples from Station 2
290 interacted differently on the chelex columns, and Ba counts were elevated (100,000
291 instead of <3,000) during analysis. Therefore we chose to not include the corresponding
292 Eu data because we cannot be certain that these analyses were not affected by a barium
293 oxide interference during ICP-MS analysis.

294 ## 3. Results

295 ### 3.1 Water Column REEs

296 Water column samples from the Oregon transit show that REE concentrations are
297 low in surface waters (13 - 20 pM Nd, 0.7 - 0.8 pM Tb, 2.8 - 4.7 pM Yb) and increase
298 with depth, characteristic of a nutrient concentration profile (**Figure 3, Appendix Table**
299 **2**). Only Nd is shown in Figure 3 as all the REE profiles are similar in shape. Our sites

300 exhibit a shallow (~250 m) subsurface REE minimum, but we do not have adequate
301 resolution to confidently identify this feature. However, we note a similar feature in prior
302 work at the Peru-Chile upwelling margin where REE concentrations at 250 m water
303 depth were less than half of the surface concentrations (Jeandel et al., 2013). Other
304 locations with a similar feature include the ocean-margin boundary off Japan where REE
305 minima occurred at ~100 m water depth (Zhang and Nozaki, 1998) and in the Bay of
306 Bengal where a REE minima was observed between ~100 m and 400 m water depth
307 (Singh et al., 2012). The shallow REE minimum off Oregon and California is similar in
308 depth (250 m) and magnitude (30 to 50% lower at minimum than surface water
309 concentrations) to the Chile upwelling margin minimum and the minimum observed in
310 the Bay of Bengal. Additionally, surface water concentrations (13 - 20 pM Nd) measured
311 off Oregon and California are comparable to the Chile margin (site UPX 26.6-27.5
312 pmol/kg Nd, Jeandel et al., 2013) and the Bay of Bengal surface waters (22-46 pmol/kg
313 Nd, Singh et al., 2012). The concentration profiles at HH1200 and HH3000 are similar
314 within the upper 600 m. Additionally the bottom waters at these sites have the highest
315 and most variable (22-43 pM Nd, 0.9-1.8 pM Tb, 7.8-9.4 pM Yb at HH1200; 12.0-38.0
316 pM Nd, 0.8-1.9 pM Tb, and 3.0-13.3 pM Yb at HH3000) dissolved REE concentrations
317 (**Figure 3)**. The near-bottom concentrations for both the HH1200 and HH3000 sites
318 approach 40 pM Nd and 2 pM Tb. There is a greater variation in bottom water HREE
319 concentrations than there is in either LREE concentrations or MREE concentrations
320 between sites HH3000 and HH1200 (13.3 pM Yb, 9.4 pM Yb respectively). The
321 difference in the water column REE profile below 600 m at sites HH1200 and HH3000
322 occurs because HH1200 has a similar change in concentration from 600 m to the bottom

323 as HH3000 has from 600m to the bottom (18 to 40 pM Nd, 1 to 2 pM Tb, 4 to ~10 pM
324 Yb) but the increase in concentration at HH1200 occurs within 600 m of water column
325 instead of 2400 m of water column at HH3000 (**Figure 3**).

326 **3.2 Pore fluid profiles**

327 The sedimentary environments of the Oregon shelf sites (Station 1, Station 2, and
328 HH200) are geochemically more homogeneous with respect to the REE concentrations
329 than the Oregon margin slope sites (HH500, HH1200, HH3000). The sediment-water
330 exchange at the deeper slope sites (HH1200 and HH3000) is likely diffusion controlled
331 whereas the shelf sites (Station 1, Station 2, HH200) are likely influenced by bioirrigation
332 and other advective factors (Severmann et al., 2010; **see 4.21**). The shelf sites (Station 1,
333 Station 2, and HH200) are characterized as having ferruginous pore fluids (values
334 typically between 50 and 250 μM, **Figure 4a and b**) indicative of anoxic sediments. In
335 contrast, the Fe profiles of the slope sites (HH500, HH1200, HH3000) change with site
336 water depth (**Figure 4c**). Specifically, the maximum concentration of Fe is greater with
337 decreasing site water depth (10 μmol/L at HH3000, 35 μmol/L at HH1200, and 70
338 μmol/L at HH500). Additionally, the first appearance of Fe occurs deeper within the core
339 at HH3000 (12 cm) than at the shallower sites (2.5 cm at HH500, 3.7 cm at HH1200)
340 (**Figure 4c**). California margin sites (Station 3, Station 6) have dissolved iron
341 concentrations up to twice the levels at any of the other sites (**Figure 4b)**. Despite this
342 difference in concentration, the shallow appearance of dissolved Fe at Station 3 and
343 Station 6 resembles the Fe profiles of the Oregon shelf sites (HH200, Station 1, Station 2;
344 **Figure 4a**). Overall, the sites in this study represent a range of geochemical conditions in
345 the pore fluids as indicated by dissolved Fe profiles.

346 A range of pore fluid REE concentration profiles also exists between the Oregon
347 shelf (Station 1, Station 2, HH200), Oregon slope sites (HH500, HH1200, HH3000), and
348 California shelf (Station 3, Station 6) sites (**Figure 4**). At each site, all pore fluid REE
349 concentration profiles have similar trends, but the concentrations vary among the REEs
350 (**Figure 4, Appendix Table 3**). For Oregon shelf sites HH200 and Station 1, REE
351 concentration profiles generally maintain uniform down-core distributions with low REE
352 concentrations (< 400 pM Nd , <15 pM Tb, and <30 pM Yb; **Figure 4a**). Station 2 is the
353 only Oregon shelf site without a uniform low REE concentration. Instead, Station 2 has a
354 deep REE concentration maximum (10.6 cm) with high REE concentrations (2250 pM
355 Nd, 60 pM Tb, 100 pM Yb). The deeper sites (HH500, HH1200, and HH3000) have
356 more REE pore fluid profile variation down-core and generally higher REE
357 concentrations (maximum pore fluid concentrations HH500: 475 pM Nd, 13 pM Tb, 25
358 pM Yb; HH1200: 500 pM Nd, 12 pM Tb, 35 pM Yb; HH3000: 790 pM Nd, 24 pM Tb,
359 62 pM Yb) (**Figure 4c**). California shelf sites (Stations 3 and 6) resemble the Oregon
360 slope sites (HH500, HH1200, and HH3000), having a shallow (~ 5 cm), subsurface REE
361 concentration maximum (850 pM Nd, 15 pM Tb, and 48 pM Yb at Station 3; and 1200
362 pM Nd, 29 pM Tb, and 58 pM Yb at Station 6) and a decrease in concentration with
363 depth (**Figure 4b**).

364 **4. Discussion**

365 **4.1 Water column REEs**

366 For comparative purposes water column samples are normalized both to Post-
367 Archean Australian Shale (PAAS) (**Figure 5a-c**) as well as to Oregon Bulk Sediment
368 (ORBS) and the Pr concentration (**Figure 5d-f**). ORBS is an average of sediment digests

from HH500, HH1200, HH3000. Here we present the REE values for ORBS that we use for normalization (**appendix Table 4; appendix text A.1**), but leave further discussion of these bulk sediment data (**appendix Table 5)** to a future publication. While the PAAS normalization is more common in the literature, the ORBS normalization provides a comparison to the local sediment source, which is important for our purposes. The double normalization using both shale and Pr concentration is applied so that the pattern variability in the lower absolute concentration samples can be compared to the patterns in the higher concentration samples. Normalization to either PAAS or ORBS removes the naturally occurring odd-even pattern in the abundance of the lanthanides (Byrne and Sholkovitz, 1996) (**Figure 5**).

Increasing REE concentrations with water depth (**section 3.1**) are accompanied by the HREE enrichment of the normalized water column REE patterns as expected for seawater (**Figure 5**) (Elderfield and Greaves, 1982; Klinkhammer 1983; Piepgras and Jacobsen, 1992; Bertram and Elderfield, 1993; German et al., 1995). The deep-water samples from HH3000 are the most HREE enriched patterns of the sites in this study (**Figure 5f**). Additionally, the greatest variation in PAAS normalized patterns coincides with site HH3000, with patterns showing the most change in terms of HREEs from the shallow water to the deep water (**Figure 5c**). Interestingly, and as discussed in section **4.23**, the deepest water column sample at HH3000 approaches the pattern of the pore fluids, and is the only sample to differ significantly from the trend of increasing HREE/LREE with increasing water depth (**Figure 5c, f**).

4.2 Pore Fluid REEs

4.21 Variability Amongst Shelf Profiles

All the Oregon shelf sites (Station 1, Station 2, HH200) appeared similar geochemically when sampled. They had bottom water O_2 from 65 to 80 μmol/L and exhibited dissolved Fe maxima in the uppermost 15 cm of the sediment column. However, the pore fluid from Station 2 was found to have much higher REE concentrations, especially at ~10 cm depth (**Figure 4a**). The REE patterns (**Figure 6b**) as well as the iron profile (**Figure 4a**) from Station 2 pore fluids provide evidence that the high REE concentrations at Station 2 (**Figure 4a**) are not a sampling artifact. With HH200 and Station 2 being positioned at approximately the same geographic location and having similar geochemical conditions, the change between high REE concentrations at Station 2 (maximum: 2248 pM Nd, 56 pM Tb, 98 pM Yb; 2007) and the low REE concentrations at HH200 (HH200 maximum: 400 pM Nd, 12 pM Tb, 22 pM Yb; 2013) suggests there could be processes causing variation in REE release from the shelf.

Spatial differences, including the patchiness of sediment distribution on the shelf, as well as temporal variability have implications as to the presence of a shelf source of REEs to the ocean. Variability in pore fluid chemical profiles has been observed in other shallow pore fluid profiles (e.g. Sholkovitz et al., 1989; Berelson et al., 2013) and possible factors include dissolved and particulate riverine REE concentrations and patterns that may change seasonally (e.g. Shiller 2002; Stolpe et al., 2013), seasonal delivery of organic carbon (e.g. Graf et al., 1983; Berelson et al., 2003), upwelling variability, bioirrigation of the sediments, or discontinuous burial creating hiatuses in sediment accumulation and differing downcore sediment properties. Additionally, the HH200 REE profile is an average profile at the site, combining the pore fluids of several

414 cores and this average is not available at Station 2, where REE profiles are from a single
415 core.

416 The mechanisms behind the observed shelf variability require further study, but
417 the observed difference in REE concentrations between 2007 (Station 2) and 2013
418 (HH200) could have implications regarding the presence and magnitude of a shelf
419 sedimentary source flux. If this variability between 2007 and 2013 is a consequence of
420 advective pore fluid transport in particular (e.g., Severmann et al., 2010) our data would
421 provide only a minimum estimate of the source flux (**see 4.3**) for these shallow sites.

422 **4.22 REEs and Fe**

423 The relationship between the REE cycling in pore fluids and Fe is not
424 straightforward. REE maximum concentrations in the pore fluids do not align with the
425 presence of dissolved Fe (**section 3.2**). Nor do the REE maximum concentrations in the
426 pore fluids align with the presence of dissolved Si or Mn (**Appendix Figure 4**). The most
427 basic interpretation of the differences in Fe and REE profiles is that Fe and REEs are not
428 as simply related as previously thought (e.g. Haley et al., 2004). The abundance of REEs
429 is much less than the abundance of Fe, meaning that the REEs could be sensitive to a
430 small change in Fe concentration, potentially below the limit of Fe detection. Another
431 possibility is that Fe and REEs are both reacting to changes in a third variable such as pH
432 or a complexing agent (e.g. Bau et al., 2013). The influence of Fe cycling on the REEs
433 cannot be fully discerned with our data set; however, Fe is nevertheless likely to be
434 important in the cycling of marine REEs (Haley et al., 2004; Bau et al., 2013; Haley et
435 al., 2013).

436 The complex relationship between Fe and REEs may be one of the reasons no
437 observable difference in pore water REE behavior was observed in our sites above,
438 within, and below the oxygen minimum zone. We expect to see elevated REE
439 concentrations with MREE enriched patterns because of the reduction of Fe-oxides in
440 anoxic sediments (Haley et al., 2004). However, the highest levels of dissolved Fe occur
441 in our shallow sites (HH200, Station 1, and Station 2 **Figure** 4) above the oxygen
442 minimum zone, and decrease from HH500 to HH1200 to HH3000. Additionally, the
443 highest REE concentrations occur at HH3000 (exception Station 2), below the oxygen
444 minimum zone. HH500 and HH1200 show no distinct REE behavior associated with the
445 overlying oxygen minimum zone. Instead, these sites appear to fit into a trend of REE
446 profile changes from shallow to deep sites that contradicts our expectations for REE
447 behavior related to the oxygen minimum zone and further supports the complex
448 relationship between the REEs and Fe. Additionally, this suggests the overlying water
449 column does not have a direct influence on pore water dynamics, possibly a result of
450 seawater REE concentrations being at least an order of magnitude lower than pore water
451 REE concentrations. Collectively, these observations suggest that iron cycling and
452 bottom water oxygen are not dominant drivers of REE behavior in these sediments.

453 **4.23 REE cycling**

454 Sediment pore fluid REE concentrations are one to two orders of magnitude
455 higher than in the overlying water column. This observation is not unique to this study
456 (e.g. Sholkovitz et al., 1989; Haley et al., 2004; Bayon et al., 2011) and implies that the
457 upper sedimentary package, via the pore fluids, is an important source of dissolved REEs
458 to the ocean (e.g. Haley et al., 2004; Schacht et al., 2010). We observe two

distinguishable pore fluid REE patterns, a HREE depleted pattern (red symbols in **Figure 6**) and a MREE and HREE enriched pattern (blue symbols in **Figure 6**). We interpret the HREE depleted pattern (red symbols in inset **Figure 6)** to be the primary diagenetic source to the pore fluids because this pattern consistently occurs at the same depth as the REE concentration maximum for all sites. The HREE depleted pattern also characterizes almost all pore fluid samples for the shallower sites (HH200, HH500, and Station 2). The HREE depleted pattern is flat across the LREEs and MREEs and begins to deviate from a straight line for the HREEs, meaning that the main difference between the primary source sediment (ORBS) and the pore fluids is in the relative abundance of HREEs. The HREE depletion (i.e., normalized values < 1) suggests that the HREEs are not as readily released from the sediments compared to the LREEs. The dominance of this HREE depleted pattern in shallow site (HH200, HH500, Station 2) pore fluids and at the depth of the maximum REE concentration at all sites implies that fractionation of the REEs continues to occur after the initial release of REEs into the pore fluid. Therefore, the source pattern is only observed in pore fluid intervals experiencing the greatest REE release from sediments ("source depth") or in pore fluids that are well mixed. As the REEs diffuse away from the source depth, both upwards and downwards, the patterns become increasingly enriched in MREEs and in HREEs (blue symbols in **Figure 6**). One possibility for this change in pattern is that the LREEs are preferentially retained within the sediment either through secondary adsorption or precipitation reactions. Consistent with the idea of LREE retention, Caetano et al. (2009) observed preferential LREE retention in a sedimentary layer that was enriched in Fe-oxyhydroxides. Another factor that could cause the HREE enrichment away from the source is the preferential

482 complexation of HREEs as they are released. This complexation then prevents the
483 HREEs from coming back out of solution as they diffuse away from the source. A
484 combination of LREE adsorption and HREE complexation can explain the increasing
485 HREE enrichment away from the source observed in pore fluid patterns.

486 The comparison of REE behavior among sites can further our understanding of
487 the mechanisms controlling the cycling of REEs, and subsequently the flux of dissolved
488 REEs from the sediments. Of the sites in this study, California shelf sites (Station 3,
489 Station 6) have more similarities with the Oregon slope sites than with the Oregon shelf
490 sites in general. Station 3 and Station 6 both have the characteristic HREE depleted
491 source patterns at the depth corresponding to the maximum concentration of REEs in
492 pore fluid (**Figure 6c,d**). Additionally, similar to Oregon slope sites HH1200 and
493 HH3000 (**Figure 6g, h**), a HREE enriched REE pattern occurs away from the source at
494 both sites.

495 Comparison of the HREE enrichment away from the source at each site also
496 contributes to our understanding of the mechanisms controlling REE cycling in pore
497 fluids. This HREE enrichment is more apparent at sites with a deeper source (i.e.,
498 HH3000), as the pore fluids from these deeper sites (i.e., HH3000) are generally more
499 enriched in the HREEs compared to the shallower, shelf pore fluids **(Figure 6 e-h).** The
500 HREE enriched pattern in pore fluids at HH3000 begins to approach the REE pattern of
501 seawater. This seawater-like HREE enrichment is not observed at the shallower sites (i.e.
502 HH500, HH200). Ultimately, the REE pattern of seawater is a function of the fluxes of
503 REEs into and out of the ocean and complexation/internal cycling of REEs within the
504 ocean. Although there are small, but measureable, differences of REE patterns in

505 seawater, the overall global consistency of the seawater REE pattern implies that internal
506 processes do not have the potential to completely change the REE pattern of seawater.
507 Therefore, a source with a more seawater like REE pattern is more logically consistent
508 with less internal alteration.

509 Of the fluxes into the ocean, the riverine REE source pattern is highly variable
510 (e.g. Shiller 2002; Stolpe et al., 2013; Sholkovitz et al., 1999; Stolpe et al., 2013) and is
511 modified significantly through estuaries (e.g. Sholkovitz, 1995; Sholkovitz and
512 Szymczak, 2000; Åström et al., 2012). REEs in submarine groundwater discharge can
513 have HREE enrichment, similar to the pattern of seawater (Johannesson et al., 2011).
514 Our data show that pore fluids also can also have a HREE enrichment, similar to the
515 pattern of seawater. This HREE enriched pattern, as seen at HH3000, may imply that
516 deep ocean pore fluids are an important REE source to the ocean. This possibility is
517 further supported by the HREE enrichment in HH3000 bottom water sample that deviates
518 from the trend observed in other deep water samples at HH3000 (**Figure 5**). This
519 deviation results in a REE pattern of HH3000 bottom water that approaches the REE
520 pattern of the upper pore fluids at HH3000 (see **section 4.1**).

521 The fundamental point from these pore fluid pattern observations is that deeper
522 sites (HH1200 and HH3000) have REE patterns that begin to appear more like seawater
523 compared to the shallower sites (Station 1, HH200, HH500). The shallower sites (Station
524 1, HH200, and HH500) maintain a HREE depletion similar to the sedimentary (pore
525 fluid) source pattern. The pore fluids at HH1200 and HH3000 demonstrate that even
526 though the REE pattern at the pore fluid concentration maximum does not resemble the
527 oceanic deep-water REE pattern, the REE pattern of the diffusive flux could resemble

528 seawater more closely because of fractionation processes preferentially taking up the
529 LREE or preferentially releasing HREEs as the REEs are transported through the pore
530 fluids.

531 **4.3 Diffusive Flux from the pore fluids**

532 Data from this as well as other studies (Elderfield and Sholkovitz, 1987;
533 Sholkovitz et al., 1989; Sholkovitz, 1992; Haley et al., 2003; Arsouze et al., 2009)
534 provides evidence that there is a large sediment (pore fluid) source of REE to the oceans.
535 Moreover, the pore fluid REE concentrations at slope sites are at least an order of
536 magnitude greater than the concentrations found in the overlying water column (**Figure**
537 **7**). Even a small addition of REEs from the sediments, when extrapolated over the area
538 of the seafloor, has the potential to significantly influence the oceanic budget of REEs.
539 Additionally, while the bottom water REE concentrations are small relative to the pore
540 fluid concentrations, these bottom water REEs are higher than the rest of the overlying
541 water column, particularly at HH1200 and HH3000 (**Figure 3**) indicating that the source
542 of REEs to the water is from below.

543 We calculated the diffusive flux of REEs to the overlying water column for the
544 Oregon slope sites (HH500, HH1200, and HH3000) that can be supported by the pore
545 water gradients. Calculations were not attempted at the shallower sites (Station 1, Station
546 2, and HH200) because these sites are likely influenced by non-diffusive processes and
547 high levels of benthic faunal activity (discussed in **4.21**) rendering these calculations
548 inappropriate for estimating sediment-water exchange rates (Archer and Devol, 1992;
549 Elrod et al., 2004; Pakhomova et al., 2007). For slope sites (HH500, HH1200, HH3000)
550 the concentration gradient of each REE in pore fluid was fit using the equation

$$C_z = C_d - (C_d - C_0)\exp(\alpha z) \quad (1)$$

where C_z is the concentration at depth, z, C_d is the concentration at infinite depth or for our purposes the approximate concentration at the source, C_0 is the concentration at the sediment-water boundary, α is the attenuation coefficient, and z is core depth in cm. This nomenclature follows that previously published for biogenic silica dissolution fluxes across the sediment water boundary (e.g., McManus et al., 1995). Fluxes across the sediment-water interface were calculated by combining Fick's first law with equation (1) resulting in the expression:

$$J = \text{Ø}D_s\alpha(C_z - C_0) \quad (2)$$

where J is the flux, Ø the estimated core top porosity and D_s the sediment diffusion coefficient corrected for tortuosity. Molecular diffusion coefficients (D) for La^{3+} at 0°C, 18°C, and 25°C and Yb^{3+} at 25°C (Li and Gregory, 1974) were used to estimate D for all REEs. D for Yb^{3+} was assumed to follow the same linear relationship between D and temperature displayed by La^{3+} allowing D values at 4°C for both elements to be calculated using the equation $D = 1 \times 10^{-7}(T) + 3 \times 10^{-6}$. A linear extrapolation from La^{3+} through Yb^{3+} resulted in the equation $Y = -1.61 \times 10^{-8}(R) + 3.42\text{x } 10^{-6}$ where R is between 1 and 14. D for each REE was assumed to be equally spaced, therefore, La was assigned R = 1 and Lu R = 14. The values for D calculated from a linear extrapolation were the same as the D values calculated using ionic radius (not shown). These calculations result in lower values of D for the HREEs than the LREEs (**Appendix Table 6**). Complexation and adsorption of REEs was not accounted for in values of D since both processes are poorly constrained in pore fluids. D_s was estimated from the relation $D_s = D/(\text{Ø}F)$ with Ø the porosity of the surface sediments (assumed = 0.9) and F

574 the formation factor. F was calculated using Archie's Law $F = \emptyset^{-n}$ (n = 2.5 for fine
575 grained sediments; Andrews and Bennett 1981, Ullman and Aller, 1982). The resulting
576 calculated fluxes (black symbols) for each REE were then normalized to ORBS and
577 PAAS (**Figure 8**). Values for C_z, C_0, α, and $\partial C/\partial z$ as well as for all REE calculated
578 fluxes are summarized in **Appendix Table 6**.
579 The profile fits could bias the flux estimates at HH500 and HH1200 because of
580 low sampling resolution above the source depth. For example, the depth resolution at
581 HH500 only allowed for flux calculations assuming linear concentration gradients in the
582 REEs. HH3000 had the most data above the source depth, implying that the model fits
583 for HH3000 are the most reliable. The calculated fluxes become systematically more
584 HREE enriched from HH500 to HH1200 to HH3000 (**Figure 8**) to the extent that at
585 HH3000 the flux is HREE enriched relative to the bulk sediment (light grey symbols).
586 The similarity of the HREE enriched flux pattern to that of the HREE enriched water
587 column is consistent with the idea that the flux from sedimentary pore fluids of the deep
588 ocean potentially has a significant influence on marine REEs.
589 Because site HH3000 exhibits a flux pattern most like seawater, and for
590 instructive purposes, we extrapolated the flux observed at HH3000 to provide a back-of-
591 the-envelope estimate of the potential global contributions of REEs from the sediment
592 (through the pore fluids) to the oceanic budget (**Table 1, Appendix A5**). This
593 extrapolation gives a global sediment flux surprisingly similar to model budget
594 requirements (Tachikawa et al. 2003; Arsouze et al., 2009) ranging between a
595 conservative estimate of 18×10^6 mol Nd yr^{-1} and a liberal estimate of 110×10^6 mol Nd
596 yr^{-1} (**Table 1**). Any value in this range suggests that the benthic flux of REEs to the ocean

597 is large, likely larger than the riverine input. A more definite estimate of the global
598 sediment contributions of REEs will require further investigation of the mechanisms,
599 applicable water depths, and role of sediment type in controlling the flux of REEs. We
600 recommend for such work efforts to improve down-core sample resolution and to access
601 flux mechanisms at shallow sites.

602 **5. Conclusions and Summary:**

603 Pore fluid REE concentrations were measured at eight sites along the Oregon and
604 California margin, adding to the limited number of pore fluid REE data to date. The
605 dissimilar dissolved Fe and REE pore fluid profiles suggest that the relationship between
606 the REEs and Fe is more complicated than discussed in Haley et al. (2004). There is a
607 clear REE pore fluid concentration maximum at most sites. The mechanism that
608 generates this sedimentary "source" of REEs remains poorly understood, but the
609 measured REE concentrations in pore fluids are at least an order of magnitude greater
610 than the concentrations in the overlying water column.

611 A HREE depleted REE pattern was characteristic of the pore fluid at the shallow
612 sites (Station 2, HH200, HH500) and of the pore fluid at the dissolved concentration
613 maximum at all sites. HREE enrichment was apparent in the REE pattern away from this
614 maximum at deep sites HH1200 and HH3000. These observed differences among the
615 REE patterns within the sediment package suggest significant alteration of the REEs as
616 they diffuse through the sediment package. Patterns appear to co-vary with REE
617 concentration suggesting that the processes influencing the REEs as they are mobilized
618 and transported through the pore fluids systematically fractionate the REEs.
619 Additionally, this fractionation may explain why the pore fluid REE patterns at deeper

sites (HH1200 and HH3000) are a closer match to the REE pattern of seawater than the REE patterns in pore fluids at shallower sites (HH200, HH500, Station 1). These data, and the resulting calculated diffusive flux of Nd from deep sediments suggest that pore fluids could be the major source of REEs to the ocean, at flux levels adequate to meet the "missing" source required by recent isotopic modeling (Arsouze et al., 2009; Tachikawa et al., 2003), making the REE flux from the sediments larger than all other oceanic REE sources, consistent with previous suggestions (e.g. Haley et al., 2003). The role of shelf sediments as a REE source is less clear, but the potential of shelf sediment pore fluid to influence oceanic REEs cannot be discounted.

Acknowledgements

Portions of this work were funded through NSF grants OCE-1147407 to JM and BH and OCE-062477 to JM, and OCE-1061218 to CR. We would like to thank the captains and crew of the R.V. *Oceanus* and the R.V. *Wecoma* for their support during various expeditions. We also appreciate many other individuals for their assistance. Chris Moser, Jesse Muratli, Paul Walczak, Chris Holm, Meghan Megowan, Nathan Ross, William Homoky, and Renee Renn helped out during the field and/or laboratory portions of this research. We also wish to acknowledge co-PIs Silke Severmann and Will Berelson for their contributions during the cruise that collected the California Margin samples. Andy Ungerer provided ICP-MS facility support at Oregon State University's W.M. Keck Collaboratory. Associate Editor Karen Johannesson, Alan Shiller, and two anonymous reviewers provided thoughtful and constructive comments that improved the text.

643
644 **References**

645 Akagi T. (2013) Rare earth element (REE)-silicic acid complexes in seawater to explain
646 the incorporation of REEs in opal and the "leftover" REEs in surface water: New
647 interpretations of dissolved REE distribution profiles. *Geochim. Cosmochim. Acta*
648 **113**, 174-192.
649 Alibo D.S. and Nozaki Y. (1999) Rare earth elements in seawater: Particle association,
650 shale-normalization, and Ce oxidation. *Geochim. Cosmochim. Acta*, **63**, 363-372.
651 Andersson P.S., Porcelli D., Frank M., Björk G., Dahlqvist R. and Gustafsson Ö. (2008)
652 Neodymium isotopes in seawater from the Barents Sea and Fram Strait Arctic-
653 Atlantic gateways. *Geochim. Cosmochim. Acta* **72**, 2854-2867.
654 Andrews D. and Bennett A. (1981) Measurement of diffusivity near the sediment-water
655 interface with a fine-scale resistivity probe. *Geochim. Cosmochim. Acta* **45**, 2169-
656 2175.
657 Archer D. and Devol, A.H. (1992) Benthic oxygen fluxes on the Washington shelf and
658 slope: A comparison of in situ microelectrode and chamber flux measurements.
659 *Limnol. Oceanogr.* **37**, 614-629.
660 Arsouze T., Dutay J.C., Lacan, F. and Jeandel, C. (2009) Reconstructing the Nd oceanic
661 cycle using a coupled dynamical—biogeochemical model. *Biogeosciences*, **6**,
662 2829-2846.
663 Åström M.E., Österholm P., Gustafsson J.P., Nystrand M., Peltola P., Nordmyr L., and
664 Boman A. (2012) Attenuation of rare earth elements in a boreal estuary. *Geochim.*
665 *Cosmochim. Acta* **96**, 105-119. doi 10.1016/j.gca.2012.08.004
666 Barnett P.R.O., Watson J. and Connely D. (1984). A multiple corer for taking virtually
667 undisturbed samples from shelf, bathyal and abyssal sediments. *Oceanologica*
668 *Acta*, **7**, 399-408.
669 Bau M. and Dulski, P. (1996) Distribution of yttrium and rare earth elements in the Penge
670 and Kuruman iron-formations, Transvaal Supergroup, South Africa. *Precambrian*
671 *Research* **79**, 37–55.
672 Bau M., Tepe N. and Mohwinkel D. (2013) Siderophore-promoted transfer of rare earth
673 elements and iron from volcanic ash into glacial meltwater, river, and ocean water.
674 *Earth Planet. Sci. Lett*. **364**, 30-36.
675 Bayon G., Birot D., Ruffine L., Caprais J.-C., Ponzevera E., Bollinger C., Donval J.-P.,
676 Charlou J.-L., Voisset M. and Grimaud, S. (2011) Evidence for intense REE
677 scavenging at cold seeps from the Niger Delta margin. *Earth Planet. Sci. Lett*.
678 **312**, 443-452.
679 Berelson W.M., McManus J., Coale K.H., Johnson K.S., Burdige D.J., Kilgore T.,
680 Colodner D., Chavez F.P., Kudela R. and Boucher J. (2003) A time series of
681 benthic flux measurements from Monterey Bay, CA. *Continental Shelf Res.* **23**,
682 457-481.
683 Berelson W.M., McManus J., Severmann, S. and Reimers C.E. (2013) Benthic flux of
684 oxygen and nutrients across Oregon/California shelf sediments. *Continental Shelf*
685 *Research,* **55**, 66-75.
686 Berger, W.H., 1976. Biogenic deep sea sediments: Production, preservation and
687 interpretation. In: Riley, J.P. and Chester, R. (eds) Chemical Oceanography,
688 Academic Press, London, NY, San Francisco, 265-388.

689 Bertram C.J. and Elderfield H. (1993) The geochemical balances of the rare earth
690 elements and neodymium isotopes in the oceans. *Geochim. Cosmochim. Acta* **57**,
691 1957-1986.
692 Byrne R.H. and Kim K.H. (1990) Rare earth element scavenging in seawater. *Geochim.*
693 *Cosmochim. Acta* **54**, 2645–2656.
694 Byrne R.H. and Sholkovitz E.R. (1996) Marine chemistry of the lanthanides. In:
695 *Handbook on the Physics and Chemistry of Rare Earths*, vol. 23 (ed. Gschneidner
696 Jr, K.A. and Eyring L.) 497-593, Elsevier.
697 Caetano M., Prego R., Vale C., de Pablo H. and Marmolejo-Rodríguez J. (2009) Record
698 of diagenesis of rare earth elements and other metals in a transitional sedimentary
699 environment. *Marine Chemistry*, **116,** 36-46. doi:10.1016/j.marchem.2009.09.003
700 Cantrell K.J. and Byrne R.H. (1987) Rare earth element complexation by carbonate and
701 oxalate ions. *Geochim. Cosmochim. Acta* **51**, 597-605.
702 Censi P., Sprovieri M., Saiano F., Di Geronimo S.I., Larocca D. and Placenti F. (2007).
703 The behaviour of REEs in Thailand's Mae Klong estuary: Suggestions from the
704 Y/Ho ratios and lanthanide tetrad effects. *Estuarine, Coastal and Shelf Science* **71**,
705 569-579.
706 De Baar J.W., German C.R., Elderfield H. and van Gaans P. (1988) Rare earth elements
707 distributions in anoxic waters of the Cariaco Trench. *Geochim. Cosmochim. Acta*
708 **52,** 1203-1219.
709 Elderfield H. (1988) The oceanic chemistry of the rare-earth elements. *Philos. Trans. R.*
710 *Soc. London* **325**, 105-126.
711 Elderfield H. and Greaves M.J. (1982) The rare earth elements in seawater. *Nature* **296**,
712 214-219.
713 Elderfield H. and Pagett R. (1986) Rare earth elements in ichthyoliths: Variations with
714 redox conditions and depositional environment. *The Science of the Total*
715 *Environment*, **49**, 175-197.
716 Elderfield H. and Scholkovitz E. (1987) Rare earth elements in the pore waters of
717 reducing nearshore sediments. *Earth Planet. Sci. Lett*. **82**, 280-288.
718 Elderfield H., Upstill Goddard R. and Sholkovitz E.R. (1990) The rare-earth elements in
719 rivers, estuaries, and coastal seas and their significance to the composition of
720 ocean waters. *Geochim. Cosmochim. Acta* **54**, 971-991.
721 Elrod V.A., Berelson W.M., Coale K.H. and Johnson K.S. (2004) The flux of iron from
722 continental shelf sediments: a missing source for global budgets. *Geophys. Res.*
723 *Lett. **31,*** doi:10.1029/2004GL020216.
724 German C.R., Masuzawa T., Greaves M.J., Elderfield H. and Edmond, J.M. (1995)
725 Dissolved rare earth elements in the Southern Ocean: Cerium oxidation and the
726 influence of hydrography. *Geochim. Cosmochim. Acta* **59**, 1551-1558.
727 Goldberg E.D., Koide M., Schmitt R.A. and Smith R.H. (1963) Rare earth distributions
728 in the marine environment. *J. Geophys. Res.* **68**, 4209-4217.
729 Goldstein S.L. and Hemming S.R. (2003) Long lived isotopic travers in oceanography,
730 paleoceanography, and ice sheet dynamics. In *Treatise on Geochemistry* (ed.
731 Elderfield, H.), Ch 6.17, Elsevier.
732 Goñi M.A., Hatten J.A., Wheatcroft R.A. and Borgeld, J.C. (2013) Particulate organic
733 matter export by two contrasting small mountainous river systems from the Pacific
734 Northwest, U.S.A. *J. Geophys. Res.: Biogeosciences*, **118**, 112-134.

735 Graf G., Schuulz R., Peinert R. and Meyer-Reil L.-A. 1983. Benthic response to
736 sedimentation events during autumn to spring at a shallow-water station in the
737 Western Kiel Bight. *Mar. Biol.* **77**, 235-246.
738 Greaves M. J., Statham P. J. and Elderfield H. (1994) Rare earth element mobilization
739 from marine atmospheric dust into seawater. *Mar. Chem*. **46**, 255–260.
740 Grenier M., Jeandel C., Lacan F., Vance D., Venchiarutti C., Cros A. and Cravatte S.
741 (2013) From the subtropics to the central equatorial Pacific Ocean: Neodymium
742 isotopic composition and rare earth element concentration variations. *J. Geophys.*
743 *Res.: Oceans*, **118**, 592-618. doi:10.1029/2012JC008239
744 Haley B.A. and Klinkhammer G.P. (2003) Complete separation of rare earth elements
745 from small volume seawater samples by automated ion chromatography: method
746 development and application to benthic flux. *Mar. Chem.* **82**, 197-220.
747 doi:10.1016/S0304-4203(03)00070-7.
748 Haley B., Klinkhammer G. and McManus J. (2004) Rare earth elements in pore waters
749 of marine sediments. *Geochim. Cosmochim. Acta* **68** (6), 1265-1279.
750 Haley B.A., Frank M., Spielhagen R.F. and Eisenhauer A. (2008) Influence of brine
751 formation on Arctic Ocean circulation over the past 15 million years. *Nat. Geo.* **1**,
752 68-71.
753 Haley B.A., Frank M., Hathorne E. and Pisias N. (2013) Biogeochemical Implications
754 from Dissolved Rare Earth Element and Nd isotope distributions in the Gulf of
755 Alaska, *Geochim. Cosmochim. Acta **126***, 455-474.
756 Hastings R.A., Goñi M.A., Wheatcroft R.A. and Borgeld J.C. (2012) A terrestrial organic
757 matter depocenter on a high-energy margin: the Umpqua River system, Oregon.
758 *Continental Shelf Res.* **39–40**, 78–91.
759 Högdahl O.T., Melsom S. and Bowen V.T. (1968) Neutron activation analysis of
760 lanthanide elements in sea water. *Adv. Chem.* **73**, 308-325.
761 Jeandel C., Delattre H., Grenier M., Pradoux C. and Lacan F. (2013) Rare earth element
762 concentrations and Nd isotopes in the Southeast Pacific Ocean. *Geochemistry*
763 *Geophysics Geosystems*, **14**, doi:10.1029/2012GC004309.
764 Johannesson K.H. and Burdige D.J. (2007) Balancing the global oceanic neodymium
765 budget: Evaluating the role of groundwater. *Earth Planet. Sci. Lett*. **253**, 129-142.
766 doi:10.1016/j.epsl.2006.10.021
767 Johannesson K.H., Chevis D.A., Burdige D.J., Cable J.E., Martin J.B. and Roy M. (2011)
768 Submarine groundwater discharge is an important net source of light and middle
769 REEs to coastal waters of the Indian River Lagoon, Florida, USA. *Geochim.*
770 *Cosmochim. Acta **75**, 825-843.*
771 Keasler K.M. and Loveland W.D. (1982) Rare earth elemental concentrations in some
772 Pacific Northwest rivers. *Earth Planet. Sci. Lett.* **61**, 68-72.
773 Kim J.-H., Torres M.E., Haley B.A., Kastner M., Pohlman J.W., Riedel M. and Lee, Y.-J.
774 (2012) The effect of diagenesis and mud migration on rare earth element
775 distribution in pore fluids of the northern Cascadia accretionary margin. *Chem.*
776 *Geol.* **291,** 152-165. doi:10.1016/j.chemgeo.2011.10.010
777 Klinkhammer G., Elderfield H. and Hudson A. (1983) Rare earth elements in seawater
778 near hydrothermal vents. *Nature* **305**, 185-188.

779 Kniskern T.A., Warrick J.A., Farnsworth K.L., Wheatcroft R.A. and Goñi M.A. (2011)
780 Coherence of river and ocean conditions along the US West Coast during storms.
781 *Continental Shelf Research* **31**, 789–805.
782 Koeppenkastrop D. and De Carlo E. H. (1993) Uptake of rare earth elements from
783 solutions by metal oxides. *Environ. Sci. Technol.* **27,** 1796 –1802.
784 Kulm L.D., Roush R.C., Harlett J.C., Neudeck R.H., Chambers D.M., and Runge E.J.
785 (1975). Oregon Continental Shelf Sedimentation: Interrelationships of Facies
786 Distribution and Sedimentary Processes. *J. of Geo.*, **83**, 145-175.
787 Kuss J., Garbe-Schonberg C.D. and Kremling K. (2001) Rare earth elements in
788 suspended particulate material of North Atlantic surface waters. *Geochim.*
789 *Cosmochim. Acta* **65**, 187–199.
790 Lacan F., Tachikawa K. and Jeandel C. (2012) Neodymium isotopic composition of the
791 oceans: A compilation of seawater data. *Chem. Geo.* **300-301**, 177-184. doi
792 10.1016/j.chemgeo.2012.01.019.
793 Lee J.H. and Byrne R.H. (1993) Complexation of trivalent rare earth elements (Ce, Eu,
794 Gd, Tb, Yb) by carbonate ions. *Geochim. Cosmochim. Acta* **57**, 295-302.
795 Leybourne M.I. and Johannesson K.H. (2008) Rare earth elements (REE) and yttrium in
796 stream waters, stream sediments and Fe-Mn oxyhydroxides: Fractionation,
797 speciation, and controls over REE + Y patterns in the surface environment.
798 *Geochim. Cosmochim. Acta* **72**, 5962-5983.
799 Li Y.H. and Gregory S. (1974) Diffusion of ions in sea water and in deep-sea sediments.
800 *Geochim. Cosmochim. Acta* **38**, 703-714.
801 Liu Y.G., Miah M.R.U. and Schmitt R.A. (1988). Cerium: A chemical tracer for paleo-
802 oceanic redox conditions. *Geochim. Cosmochim. Acta* **52**, 1361-1371.
803 Lyle M., Mix A., Ravelo A.C., Andreasen D., Heusser L., Olivarez A. (2000) Millennial-
804 scale $CaCO_3$ and C_{org} events along the northern and central California margins:
805 stratigraphy and origins. In: Lyle, M., Koizumi, I., Richter, C., Moore, Jr., T.C.
806 (Eds.), *Proceedings of the Ocean Drilling Program, Scientific Results*, College
807 Station, TX.
808 Martin J.M., Høgdahl O. and Philippot J.C. (1976) Rare Earth Element Supply to the
809 Ocean. *J. Geophys. Res.* **81,** 3119-3124.
810 McManus J., Berelson W.M., Hammond D.E., Kilgore T.E., Ragueneau O.G., DeMaster
811 D.J. and Collier R.W. (1995) Early diagenesis of biogenic silica: Dissolution rates,
812 kinetics, and paleoceanographic implications. *Deep Sea Res.* **42**, 871-903.
813 McManus J., Berelson W.M., Severmann S., Johnson K.S., Hammond D.E., Roy M. and
814 Coale K.H. (2012) Benthic manganese fluxes along the Oregon-California
815 continental shelf and slope, *Continental Shelf Research*, **43**, 71-85.
816 Menard H.W. and Smith S.M. (1966) Hypsometry of Ocean Basin Provinces. *J.*
817 *Geophys. Res.* **71**, 4305-4325.
818 Moffett J.W. (1990) Microbially mediated cerium oxidation in sea water. *Nature*, **345**,
819 421-423.
820 Nance W. B. and Taylor S. R. (1976) Rare earth element patterns and crustal evolution—
821 I. Australian post-Archean sedimentary rocks. *Geochim. Cosmochim. Acta* **40,**
822 1539–1551.
823 Oka A., Hasumi H., Obata H., Gamo T. and Yamanaka Y. (2009) Study on vertical
824 profiles of rare earth elements by using an ocean general circulation model.

Global Biogeochem. Cycles **23**, doi:10.1029/2008GB003353
Pakhoma S.V., Hall P.O.J., Kononets M.Y., Rozanov A.G., Tengberg A. and Vershinin A.V. (2007) Fluxes of iron and manganese across the sediment-water interface under various redox conditions. *Mar. Chem.* **107,** 319-333.
Palmer M.R. and Elderfield H. (1986) Rare earth elements and neodymium isotopes in ferromanganese oxide coatings of Cenozoic foraminifera from the Atlantic Ocean. *Geochim. Cosmochim. Acta* **50**, 409-417.
Pearce C.R., Jones M.T., Oelkers E.H., Pradoux C. and Jeandel C. (2013) The effect of particulate dissolution on the neodymium (Nd) isotope and Rare Earth Element (REE) composition of seawater. *Earth Planet. Sci. Lett*. **369-370,** 138-147. (doi:10.1016/j.epsl.2013.03.023).
Piepgras D.J. and Jacobsen S.B. (1992) The behavior of rare earth elements in seawater: Precise determination of variations in the North Pacific water column. *Geochim. Cosmochim. Acta* **56**, 1851-1862.
Roy M., McManus J., Goñi M.A., Chase Z., Borgeld J.C., Wheatcroft R.A., Muratli J.M., Megowan M.R. and Mix A. (2013) Reactive iron and manganese distributions in seabed sediments near small mountainous rivers off Oregon and California, (USA). *Continental Shelf Research* **54**, 67-69. http://dx.doi.org/10.1016/j.csr.2012.12.012
Schacht U., Wallmann K. and Kutterolf S. (2010) The influence of volcanic ash alteration on the REE composition of marine pore waters. *J. Geochem. Explorations* **106**, 176-187.
Scher H.D. and Martin E. (2004) Circulation in the Southern Ocean during the Paleogene inferred from neodymium isotopes. *Earth and Planet Sci. Lett.* **228**, 391-405.
Schijf J. and Byrne R.H. (2004) Determination of $SO_4\beta_1$ for yttrium and the rare earth elements at I =0.66 m and t =25°C- Implications for YREE solution speciation in sulfate-rich waters. *Geochim. Cosmochim. Acta* **68**, 2825-2837.
Severmann S., McManus J., Berelson W.M. and Hammond D.E. (2010) The continental shelf benthic iron flux and its isotope composition. *Geochim. Cosmochim. Acta* **74**, 3984–4004.
Sherrell R.M., Field M.P. and Ravizza G. (1999) Uptake and fractionation of rare earth elements on hydrothermal plume particles at 9°25'N, east Pacific Rise. *Geochim. Cosmochim. Acta* **63,** 1709-1722.
Shiller A.M. (2002) Seasonality of dissolved rare earth elements in the lower Mississippi River. *Geochem. Geophy. Geosys*. **3(11)**. doi:10.1029/2002GC000372
Sholkovitz E.R. (1990) Rare earth elements in marine sediments and geochemical standards. *Chem. Geol*. **88**, 333-347.
Sholkovitz E. (1992) Chemical evolution of rare earth elements: fractionation between colloidal and solution phases of filtered river water. *Earth Planet. Sci. Lett.* **114**, 77–84.
Sholkovitz E.R. (1995) The aquatic chemistry of rare earth elements in rivers and estuaries. *Aquatic Geochem.*, **1**, 1-34.
Sholkovitz E.R. and Schneider D.L. (1991). Cerium redox cycles and rare earth elements in the Sargasso Sea. *Geochim. Cosmochim. Acta* **55**, 2737-2743.

869 Sholkovitz E. and Szymczak R. (2000). The estuarine chemistry of rate earth elements:
870 comparison of the Amazon, Fly, Sepik and the Gulf of Papua systems. *Earth*
871 *Planet. Sci. Lett.* **179**, 299-309.
872 Sholkovitz E.R., Piepgras D.J. and Jacobsen S.B. (1989) The pore water chemistry of rare
873 earth elements in Buzzards Bay sediments. *Geochim. Cosmochim. Acta* **53**, 2847-
874 2856.
875 Sholkovitz E.R., Landing W.M. and Lewis B.L. (1994) Ocean particle chemistry: the
876 fractionation of rare earth elements between suspended particles and seawater.
877 *Geochim. Cosmochim. Acta* **58**, 1567–1579.
878 Sholkovitz E.R., Elderfield H., Szymczak R. and Casey K. (1999) Island weathering:
879 river sources of rare earth elements to the Western Pacific Ocean. *Mar. Chem.* **68**,
880 39-57.
881 Singh S.P., Singh S.K., Goswami V., Bhushan, R. and Rai V.K. (2012) Spatial
882 distribution of dissolved neodymium and ε_{Nd} in the Bay of Bengal: Role of
883 particulate matter and mixing water masses. *Geochim. Cosmochim. Acta* **94**, 38-
884 56. doi 10.1016/j.gca.2012.07.017
885 Sommerfield C.K. and Nitrouer C.A. (1999) Modern accumulation rates and a sediment
886 budget for the Eel shelf: a flood-dominated depositional environment. *Mar. Geol.*
887 **154**, 227-241.
888 Stolpe B., Guo L. and Shiller A.M. (2013) Binding and transport of rare earth elements
889 by organic and iron-rich nanocolloids in Alaskan rivers, as revealed by field-flow
890 fractionation and ICP-MS. *Geochim. Cosmochim. Acta* **106**, 446-462.
891 Tachikawa K., Jeandel C. and Roy-Barman M. (1999) A new approach to the Nd
892 residence time in the ocean: the role of atmospheric inputs. *EPSL*, **170**, 433-446.
893 Tachikawa K., Athias V. and Jeandel, C. (2003) Neodymium budget in the ocean and
894 paleoceanographic implications. *J. Geophys. Res*. **108**, 3254.
895 Doi:10.1029/1999JC000285.
896 Tang J. and Johannesson K.H. (2010) Rare earth elements adsorption onto Carrizo sand:
897 Influence of strong solution complexation. *Chem. Geol.* **279**, 120-133.
898 Ullman W.J. and Aller R.C. (1982) Diffusion coefficients in nearshore marine
899 sediments. *Limnol. Oceanogr.* **27**, 552-556.
900 Van de Flierdt T., Frank M., Lee D.-C., Halliday A.N., Reynolds B.C. and Hein J.R.
901 (2004) New constraints on the sources and behavior of neodymium and hafnium
902 in seawater from Pacific Ocean ferromanganese crusts. *Geochim. Cosmochim.*
903 *Acta* **68**, 3827-3843.
904 VanLaningham S., Duncan R.A., Pisias N.G., and Graham D.W. (2008) Tracking fluvial
905 response to climate change in the Pacific Northwest: a combined provenance
906 approach using Ar and Nd isotopic systems on fine-grained sediments. *QSR*, **27**,
907 497-517.
908 Wetz M.S., Hales B., Wheeler P.A., Chase Z. and Whitney M. (2006) Riverine input of
909 macronutrients, iron and organic matter to the coastal ocean off Oregon, USA,
910 during winter. *Limnol. Oceanogr.* **5,** 2221-2231.
911 Wheatcroft R.A. and Sommerfield C.K. (2005) River sediment flux and shelf sediment
912 accumulation rates on the Pacific Northwest margin. *Continental Shelf Research*
913 **25**, 311–332.
914 Wheatcroft R.A., Goñi M.A., Richardson K.N. and Borgeld J.C. (2013) Natural and

915 human impacts on centennial sediment accumulation patterns on Umpqua River
916 margin, Oregon. *Mar. Geol.* **339**, 44-56.
917 Zhang J. and Nozaki Y. (1998) Behavior of rare earth elements in seawater at the ocean
918 margin: A study along the slopes of Sagami and Nankai troughs near Japan.
919 *Geochim. Cosmochim. Acta* **62,** 1307-1317.

Figure Captions for:

The sedimentary flux of dissolved rare earth elements to the ocean

Figure 1 Site locations. Filled symbols represent sites unique to this study and open symbols are sites where we have analyzed archived samples from prior expeditions (see text). Rivers are indicated in black and labeled. The Eel River flows into the southern edge of this map and is not shown.

Figure 2 Water column oxygen, temperature, and salinity. (a) Dissolved oxygen, **(b)** Salinity, and **(c)** Temperature as a function of water depth. Profile data are taken from the HH3000 study site. Symbols for other locations denote sampling depths, and the symbols are placed along the oxygen profile for illustrative purposes, see **Appendix Table 1** for bottom water oxygen values.

Figure 3 Water column Nd concentration. Water column Nd concentration plotted as a function of water depth for Oregon slope sites. Uncertainties are ± 1 σ based on sample replicates. Our internal standards, "NBP" samples are placed in the box at the base of the figure with their average concentration ± 1 σ. Samples for the upper water column at HH500 were not collected. NBP samples are large volume filtered seawater samples collected from the Bransfield Strait in 1995 and acidified to pH 2.5 from water depths of 1310 m (NBPGSR10), 1152 m (NBP 1152), and 1097 m (NBP 1097).

Figure 4 Pore water profiles. Dissolved rare earth element (Nd, Tb, and Yb) and iron plotted against sediment depth in pore fluids from (**a**) the Oregon shelf, (**b**) the California shelf, and (**c**) the Oregon slope. For station 2, Nd concentrations peak at 2250 pM (not shown) and Yb concentrations peak at 98 pM (not shown).

Figure 5 Water column REE patterns. (a – c) Water column profile rare earth elements normalized to PAAS (values after Nance and Taylor 1976) grouped according to the stations. The data is color-coded to capture the water depth information (see legend). **(d – e)** Water column profile rare earth elements for the same samples as plotted in (a – c) but with the normalization now calculated for ORBS and Pr. Bottom water is shown in black (gray in color version) for all plots. The reader is referred to the web version of this article for interpretation of the color version of this figure. PAAS values used La: 273.6; Ce: 570.9; Pr: 63.2; Nd: 221.9; Sm: 35.2; Eu: 7.2; Gd: 29.9; Tb: 4.5; Dy: 27.1; Ho: 6.1; Er: 17.3; Tm: 2.4; Yb: 15.4; Lu: 2.5. ORBS values used La: 17.12; Ce: 33.61; Pr: 4.03; Nd: 16.10; Sm: 3.43; Eu: 0.89; Gd: 3.14; Tb: 0.48; Dy: 3.08; Ho: 0.60; Er: 1.81; Tm: 0.26, Yb: 1.72; Lu 0.30.

Figure 6 Pore water REE patterns. Pore fluid REE patterns normalized to ORBS and Pr for **(a)** Station 1, **(b)** Station 2, **(c)** Station 3, **(d)** Station 6, **(e)** HH200, **(f)** HH500, **(g)** HH1200, and **(h)** HH3000. Each pattern represents a different depth interval from the site. Patterns that have a lower HREE:LREE than ORBS are plotted in red and patterns with the highest HREE:LREE are in blue. Intermediate patterns are in light gray. Inset Pr profile for each site with color corresponding to pattern line for each depth. Thick gray bars in inset represent zone of maximum concentration for sites HH1200 and HH3000, gray lines mark every 5 cm of core depth in the inset Pr profile. The reader is referred to the web version of this article for interpretation of the color referenced in this figure.

Figure 7 Water column pore fluid composite Nd profile. Water column and pore water Nd plotted as a function of water depth for **(a)** HH500, **(b)** HH1200, and **(c)** HH3000.

The gray box indicates sediment and 1σ error bars are smaller than symbol size. Note that the sediment depth scale (gray area) and the water column depth portion of the scale differ.

Figure 8 REE flux patterns. **(a)** HH500 calculated flux patterns normalized to PAAS and Pr, **(b)** HH1200 calculated flux patterns normalized to PAAS and Pr, **(c)** HH3000 calculated flux patterns normalized to PAAS and Pr, **(d)** HH500 calculated flux patterns normalized to ORBS and Pr, **(e)** HH1200 calculated flux patterns normalized to ORBS and Pr, **(f)** HH3000 calculated flux patterns normalized to PAAS and Pr. Bulk sediment shown is by site and is not ORBS. Pore water average is also site specific. The REE pattern of the calculated flux is shown in black, the average pore water REE pattern in gray and the bulk sediment REE pattern in light gray. Symbols are site specific.

Table 1 Source Comparison. Oceanic Nd source fluxes and extrapolated neodymium flux out of the deep sediments. The calculated flux is similar to the missing flux from models. The missing sediment source, riverine source, and atmospheric source are taken from Arsouze et al. 2009. Submarine groundwater discharges are from Johannesson and Burdige 2007. Seafloor areas and province are from Menard and Smith 1966. Sediment coverage estimated from Berger 1976. All flux values shown are based on an extrapolation using the flux from site HH3000 (32 pmol cm^{-2} yr^{-1}), additional flux extrapolations using the flux from site HH500 (13 pmol cm^{-2} yr^{-1}) are provided in **Appendix table 7**. Details of flux extrapolation are provided in **Appendix A5** and complete list of flux calculations in **Appendix tables 6 and 7**.

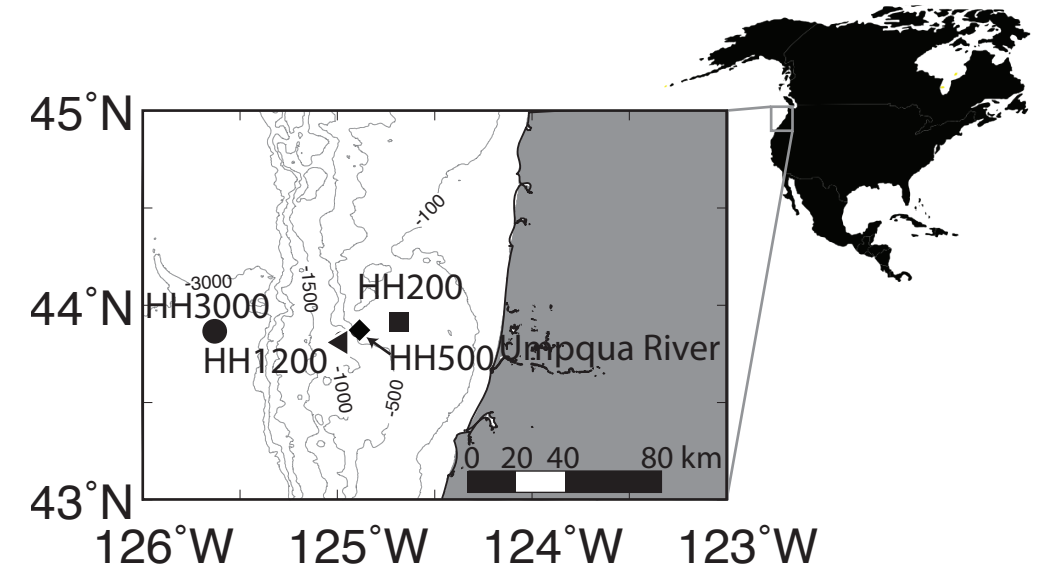
45˚N
44˚N
43˚N
126˚W
125˚W
124˚W
123˚W
-100
-3000
-1500
-1000
-500
HH3000
HH200
HH1200
HH500
Umpqua River
0 20 40 80 km

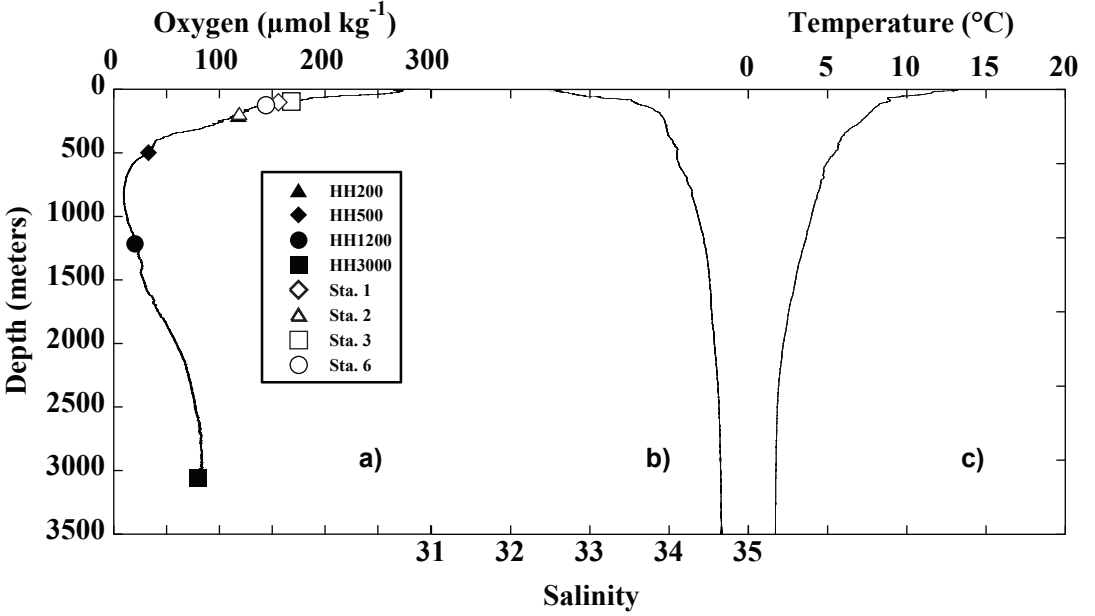
Oxygen (µmol kg-1)
0
100
200
300
Temperature (°C)
0
5
10
15
20
Depth (meters)
0
500
1000
1500
2000
2500
3000
3500
HH200
HH500
HH1200
HH3000
Sta. 1
Sta. 2
Sta. 3
Sta. 6
a)
b)
c)
31
32
33
34
35
Salinity

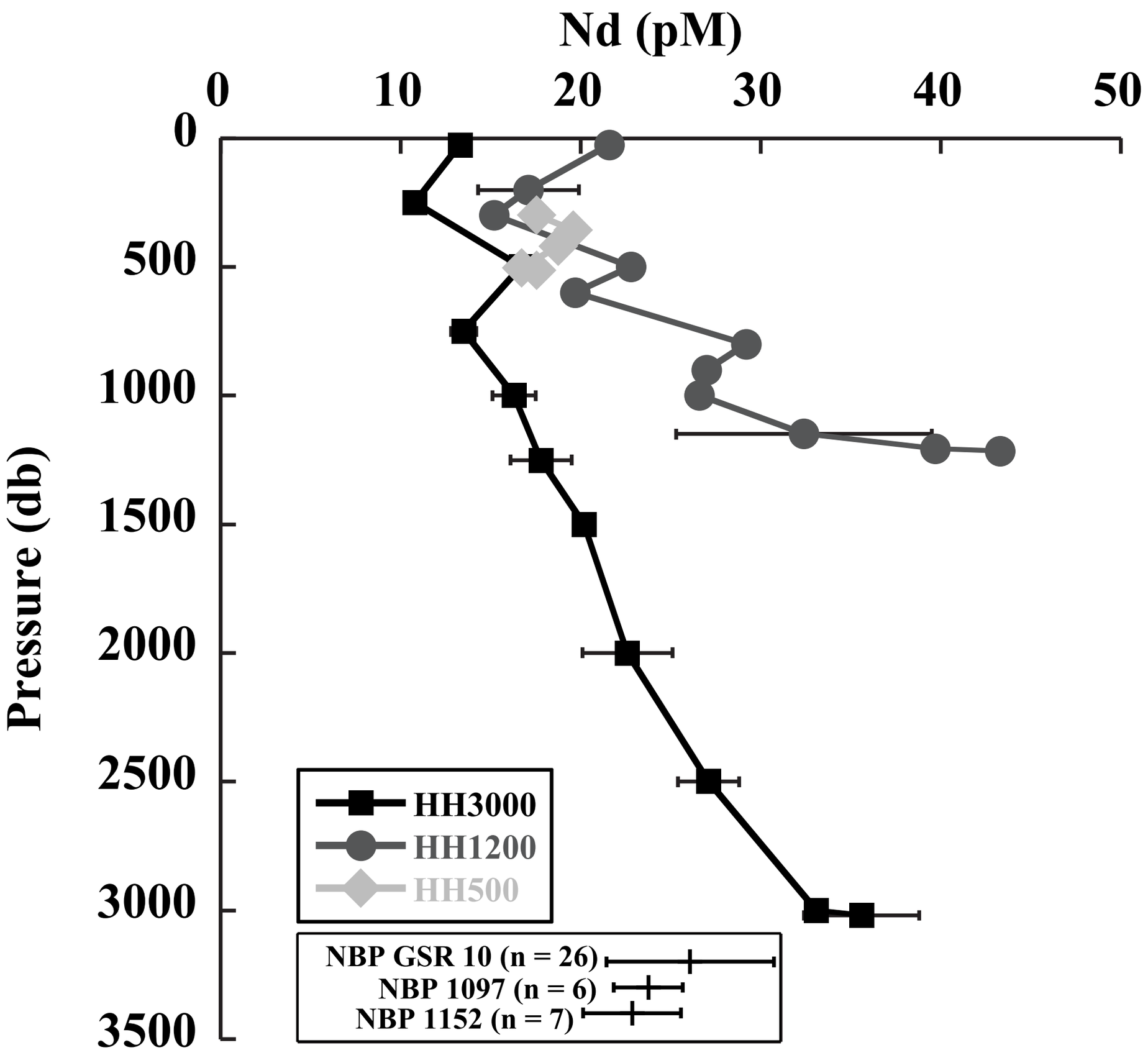
Nd (pM)
0
10
20
30
40
50
Pressure (db)
0
500
1000
1500
2000
2500
3000
3500
HH3000
HH1200
HH500
NBP GSR 10 (n = 26)
NBP 1097 (n = 6)
NBP 1152 (n = 7)

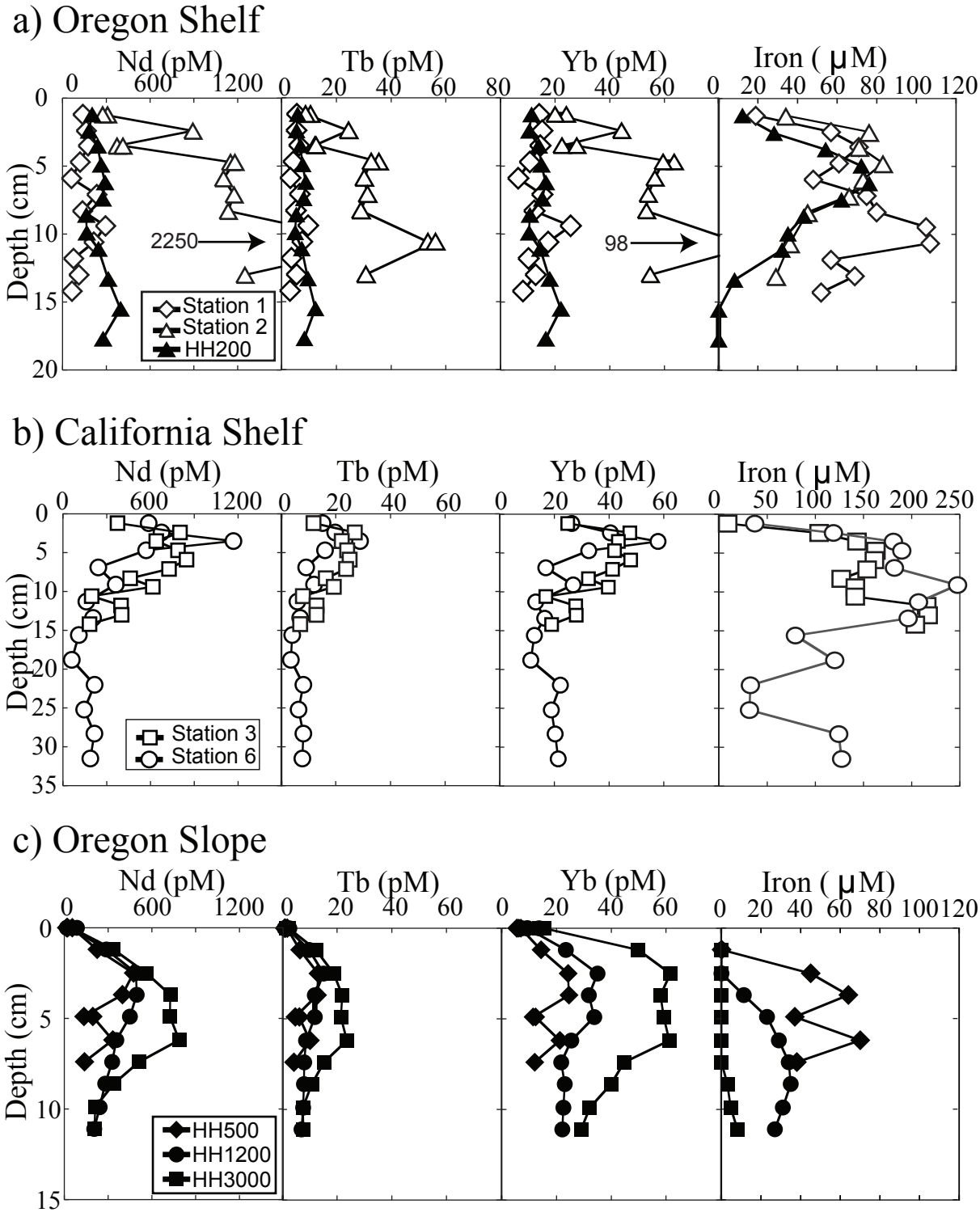
a) Oregon Shelf
Nd (pM)
Tb (pM)
Yb (pM)
Iron (μM)
Depth (cm)
2250
98
Station 1
Station 2
HH200
b) California Shelf
Station 3
Station 6
c) Oregon Slope
HH500
HH1200
HH3000

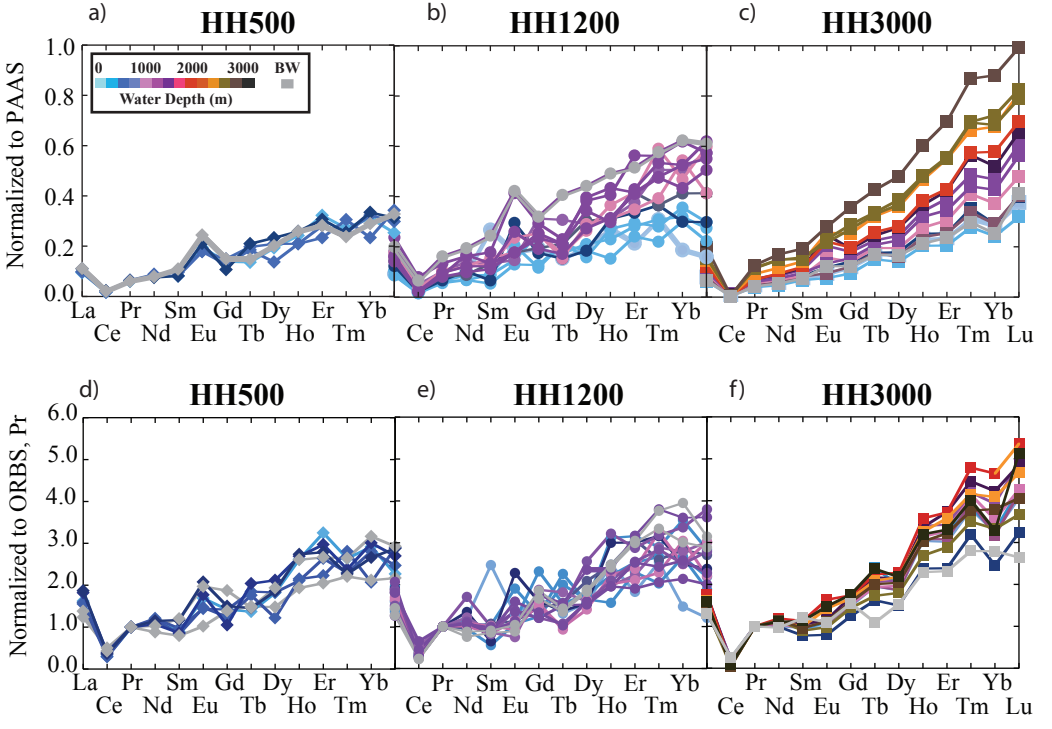
a)
HH500
b)
HH1200
c)
HH3000
0
1000
2000
3000
BW
Water Depth (m)
Normalized to PAAS
1.0
0.8
0.6
0.4
0.2
0.0
La Ce Pr Nd Sm Eu Gd Tb Dy Ho Er Tm Yb
Pr Ce Sm Nd Gd Eu Dy Tb Er Ho Yb Tm
Pr Ce Sm Nd Gd Eu Dy Tb Er Ho Yb Tm Lu
d)
HH500
e)
HH1200
f)
HH3000
Normalized to ORBS, Pr
6.0
5.0
4.0
3.0
2.0
1.0
0.0
La Ce Pr Nd Sm Eu Gd Tb Dy Ho Er Tm Yb
Pr Ce Sm Nd Gd Eu Dy Tb Er Ho Yb Tm
Pr Ce Sm Nd Gd Eu Dy Tb Er Ho Yb Tm Lu

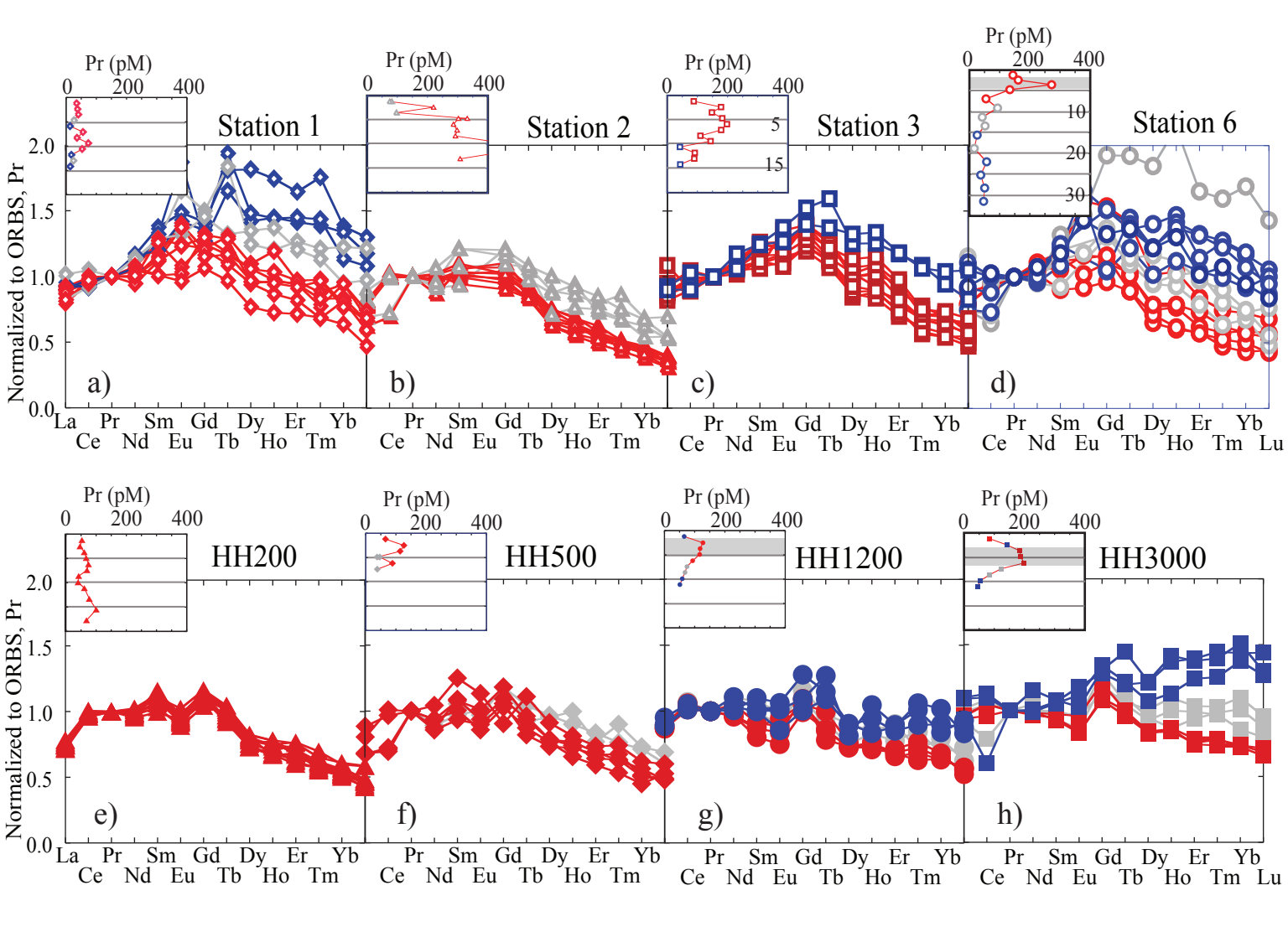
Station 1
Station 2
Station 3
Station 6
HH200
HH500
HH1200
HH3000
Pr (pM)
0
200
400
5
15
10
20
30
Normalized to ORBS, Pr
0.0
0.5
1.0
1.5
2.0
a)
b)
c)
d)
e)
f)
g)
h)
La Pr Sm Gd Dy Er Yb
Ce Nd Eu Tb Ho Tm
Lu

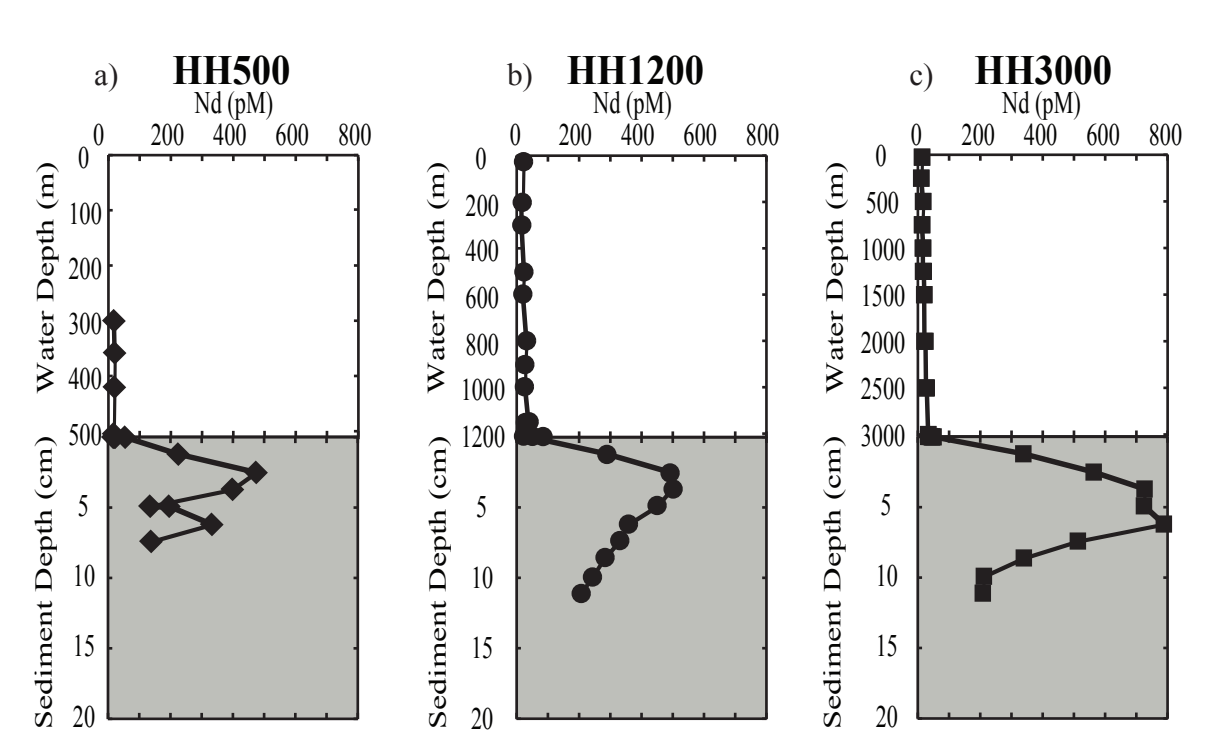
a)
HH500
Nd (pM)
0
200
400
600
800
Water Depth (m)
0
100
200
300
400
500
Sediment Depth (cm)
5
10
15
20
b)
HH1200
Nd (pM)
0
200
400
600
800
Water Depth (m)
0
200
400
600
800
1000
1200
Sediment Depth (cm)
5
10
15
20
c)
HH3000
Nd (pM)
0
200
400
600
800
Water Depth (m)
0
500
1000
1500
2000
2500
3000
Sediment Depth (cm)
5
10
15
20

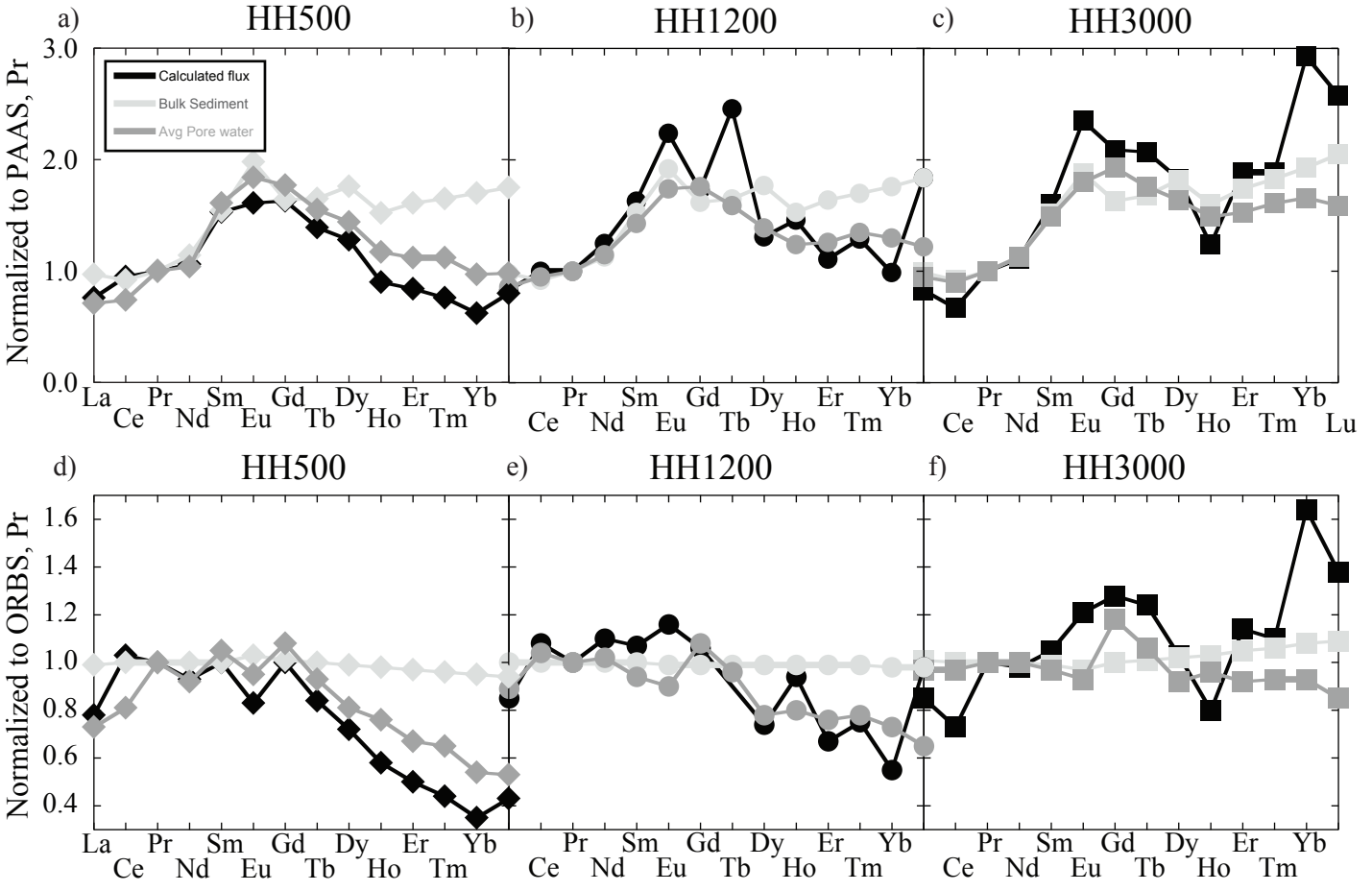
a)
HH500
b)
HH1200
c)
HH3000
Calculated flux
Bulk Sediment
Avg Pore water
Normalized to PAAS, Pr
3.0
2.0
1.0
0.0
La Ce Pr Nd Sm Eu Gd Tb Dy Ho Er Tm Yb Lu
d)
HH500
e)
HH1200
f)
HH3000
Normalized to ORBS, Pr
1.6
1.4
1.2
1.0
0.8
0.6
0.4

Oceanic Nd Source Fluxes		Flux out of Deep Sediments (10^6mol Nd yr^{-1})			
Source	10^6mol Nd yr^{-1}	Area (10^6 km^2)	Full Area	No Calcareous	Only Pelagic
Rivers	1.8	151.5 Abyssal plains/hills	48	37	18
Atmospheric	0.7	170.8 plus continental rise	54	40	21
Sediment Dissolution modeled as misssing	76	289.6 plus oceanic rise & ridge	92	64	35
Submarine Groundwater Discharge	29-81	344.8 plus continental slope & shelf	110	73	42

Supporting online material for:

The sedimentary flux of dissolved rare earth elements to the ocean

Tables 1-3 present site descriptions (1), REE concentrations in seawater (2) and REE concentrations in pore fluids (3) and are discussed in the main text.

A.1 ***Oregon Bulk Sediment (ORBS)***

ORBS is the average REE pattern of the total sediment digests from sites HH500, HH1200, and HH3000 (**Appendix Table 4**). Sediments from HH200, HH500, HH1200, and HH3000 were digested in a mixture of HNO_3, HCl and HF using a CEM Corp MARS-5 microwave following the procedures of Muratli et al. (2012) and analyzed for REEs on the Thermo VG ExCell quadropole ICP-MS at the W.M. Keck Laboratory. The sediment intervals analyzed correspond to the same depth intervals as the pore fluids. The REEs in these sediments are largely invariant (**Appendix Table 5**). The patterns from all measured intervals at each site were averaged into a site average REE pattern, and then the three average site profiles were averaged to obtain ORBS (**Appendix Table 4**). The REE pattern of ORBS normalized to PAAS is shown in **Appendix Figure 1**.

A.2 ***Rhizons and Rare Earth Elements***

Laboratory experiments with REE enriched seawater were run to test the impact of rhizons on the extraction of REEs from pore fluids. For both tests, a known REE spike (0.15 ng (**Figure A2 a**) and 0.05 ng (**Figure A2 b**)) was added to a filtered, unacidified surface seawater sample from the Gulf of Mexico. Syringes and Rhizons used in this

experiment were the same type as the ones used at sea for pore water collection. The spiked solution was pulled through a Rhizon and analyzed for REE concentrations. Additionally, the spiked solution was collected in a syringe and analyzed for REE concentrations without passing through a Rhizon to establish a syringe blank.

Results from the Rhizon tests were variable. In the higher concentration experiments, the cleaned Rhizon showed LREE blanks as high as ~4x the loaded concentration (**Figure A2 a**) and the unclean Rhizon up to ~2x the spike concentration. MREE and HREE depletion (>50%) was observed with both clean and uncleaned (new) Rhizons. However, one of the uncleaned Rhizon tests displayed no MREE or HREE depletion, highlighting the erratic nature of the problem with Rihzons. These results imply that Rhizons should probably not be used to collect samples for REE concentration determination. All results presented in this manuscript are from pore water samples collected using centrifuge techniques (as described in **2.2**).

A.3 *Chelex Columns and Seafast II*

REE concentrations were analyzed after being separated from the seawater matrix either through the use of Chelex-resin columns or an ESI seaFAST II system. Samples were run by both methods to check the reproducibility between methods (**Figure A3)**. Repeatability between methods can be seen with both pore water and seawater samples. The deviation of the Oct-Chelex interval samples (solid lines) is due to the poor preservation of HREEs in solution at pH 2.5 as discussed below. When the same samples were processed using Chelex at the time of seaFAST II analysis (July Chelex) the results from each method were in agreement.

A.4 *Acidification and Rare Earth Element Preservation*

Pore water and seawater samples from HH200, HH500, HH1200, and HH3000 were acidified to pH 2.5 at the time of collection and analyzed for rare earth element concentrations within one month of collection. This degree of acidification appears adequate for maintaining rare earth elements in solution for seawater samples, however a lower pH is needed for pore water fluids. For example, the HH1200 pore fluids were run again 9 months after collection and showed up to a 60% loss of heavy rare earth elements from solution (**Figure A3**). In some cases, loss was also observed in the middle rare earths starting at Sm. Ce was the only element showing a concentration increase (30-40% in pore water) over the same 9 month time span. The rest of the light rare earth elements did not show any change. These REE concentration changes in pore water make a significant impact on the shape of the pattern of the rare earth elements when normalized to PAAS (**Figure A3 b**).

BIF samples were acidified to pH 1.7 and analyzed for rare earth element concentrations The REE patterns from BIF II sites 1, 2, 3, and 6 fall within the observed range of pore water patterns from HH200, HH500, HH1200, and HH3000. The agreement among the BIF II patterns (samples preserved at pH 1.7) and the samples run shortly after collection suggests that pH 1.7 is adequate to preserve the HREEs in solution and these patterns are assumed accurate but further testing is needed to confirm that no MREE or HREE loss occurs at pH 1.7 in pore water. It is clear that as samples are stored for prolonged periods at higher pH (~2.5) they may be subject to HREE loss from solution. We do not know to what degree our samples may have been affected by

REE removal from solution, but the general agreement and consistency among our results suggest that this effect is minor in our data set.

A.5 *Flux calculations*

To better understand the implications of the calculated flux at HH3000, we extrapolated the HH3000 flux (section **4.3**) to larger areas of the ocean using province and sediment type restrictions. Province areas (Menard and Smith, 1966) considered were the abyssal hills and plains (mainly between 3000 and 6000 km water depth), the continental rise (mainly between 2000 and 5000 km water depth), the oceanic rise and ridge (mainly between 2000 and 6000 km water depth), and the continental slope and shelf (mainly shallower than 2000 km water depth) (Menard and Smith, 1966; **Table 1, Appendix Table 6, Appendix Table 7**). To provide a more conservative estimate, we applied sediment restrictions to constrain these areas. We removed the area of the ocean floor covered by calcareous ooze (because of the low Nd abundance in carbonate sediments; e.g. Parekh et al., 1977; Elderfield et al., 1981; Shaw and Wasserburg, 1985). by assuming an average carbonate compensation depth (CCD) of 5000 m, so that 50% of OCBN and 20% of RISE could not be calcareous. The remaining areas were considered to be 47% calcareous (Berger, 1976). For our most conservative estimate, we constrained the province areas with a pelagic sediment requirement, calculating fluxes based on 38% of the original province areas (Berger, 1976) for a rough estimate of the flux possible from only pelagic sediments (**Table 1, Appendix Table 6, Appendix Table 7**).

From these extrapolations, the sedimentary source of dissolved REE appears to be a significant contributor to the global REE budget. While we base these extrapolations on our best-constrained flux estimate (HH3000, flux of ~32 pmol cm^{-2} yr^{-1}) this flux value is

similar to the flux estimated at HH1200 (38 pmol cm^{-2} yr^{-1}) and the same order of magnitude as the flux estimated at HH500 (13 pmol cm^{-2} yr^{-1})(**Appendix Table 6)**. Because of the sampling resolution, we used a linear concentration-depth gradient at HH500; the same linear slope applied to HH1200 and HH3000 resulted in similarly lower fluxes at these sites (14 pmol cm^{-2} $yr^{-}1$, 13 pmol cm^{-2} yr^{-1} respectively, **Appendix Table 6)**. Importantly, the range of our calculated flux estimates (Appendix Table 7) is relatively small (8 to 110x10^{6} mol Nd yr^{-1}) considering the high uncertainty in these global extrapolations.

Supporting online material references

Berger, W.H., 1976. Biogenic deep sea sediments: Production, preservation and interpretation. In: Riley, J.P. and Chester, R. (eds) Chemical Oceanography, Academic Press, London, NY, San Francisco, pp 266-388.

Elderfield H., Hawkesworth C.J., Greaves M.J. and Calvert S.E. (1981) Rare earth element geochemistry of oceanic ferromanganese nodules and associated sediments. *Geochim. Cosmochim. Acta*, **45**, 513-528.

Muratli J.M., McManus J., Mix, A. and Chase Z. (2012) Dissolution of fluoride complexes following microwave-assisted hydrofluoric acid digestion of marine sediments. *Talanta* **89**, 195–200. doi:10.1016/j.talanta.2011.11.081.

Parekh P.R., Moller P., Dulski P. and Bausch W.M. (1977) Distribution of trace elements between carbonate and non-carbonate phases of limestone. *Earth Planet. Sci. Lett.,* **34,** 39-50.

Shaw H.F. and Wasserburg G.J. (1985) Sm-Nd in marine carbonate and phosphorites: Implications for Nd isotopes in seawater and crustal ages. *Geochim. Cosmochim. Acta*, **49**, 503-518.

Supporting Online Material Figure Captions for:
The sedimentary flux of dissolved rare earth elements to the ocean

Figure A1 ORBS REE normalized to PAAS. REE pattern of Oregon Bulk Sediment (ORBS) normalized to PAAS.

Figure A2 Rhizon REEs. Results of rhizon yield test with known REE spike. (**a**) REEs measured after (**a**) a 0.15ng REE spike and (b) a 0.05ng REE spike was passed through a clean rhizon (green diamonds), uncleaned rhizon (blue triangle), and the control, no rhizon (pink circle).

Figure A3 REE Preservation. Comparison of REEs measured using Chelex column chromatography and REEs measured using the ESI SeaFast II system in the Keck Laboratory at Oregon State University. Chelex columns were measured in October (solid line) and July (triangles), SeaFast II measurements were only taken in July (squares). All samples represented here were stored at pH 2.5 (**a**) Seawater values were reproducible between methods and remained constant between sample times. (**b**) Pore water values were reproducible between methods but changed over time indicating that pH 2.5 is not low enough for REE preservation in pore water samples.

Figure A4 Additional Pore Fluid Profiles. Nd, Si (open black diamond), P (pink circle), Mn (green square), Fe (orange triangle), Yb:Pr and Gd:Pr profiles for all sites, as available. Mn data was below detection at sites HH200, HH500, and HH1200. Mn data for stations 1, 2, 3, and 6 is provided in **Appendix Table 3** but is not shown here, as it would be indistinguishable from zero on the given scale. Nd and REE ratio symbols vary by site to match **Figure 4**; Yb:Pr shown in gray, Gd/Pr in black. All REE ratio calculations made on ORBS-normalized REE values.

Table A1 Site Descriptions. Water depth, cruise ID, sampling date, latitude, longitude, and bottom oxygen for each site. Bottom water oxygen for HH200, HH500, HH1200, and

HH3000 from CTD measurement; bottom water oxygen for Stations 1, 2, 3, and 6 are from discrete measurements.

Table A2 Oregon Slope Water Column REEs. Water column REE concentrations in pM for HH500, HH1200, and HH3000. Samples above 300 m at HH500 were not collected. The mean REE concentrations of NBPGSR10 (27 measurements) and procedural blank are reported with 1σ error.

Table A3 Pore water centrifuge results. Fe and Mn concentrations for all sites reported in μmol/L. REE concentrations for all sites reported in pM. Si and P concentrations reported in μmol/L where available. Depth 0.0 is bottom water collected from niskin bottle attached to multicorer. A "*" next to 0.0 denotes an unfiltered sample, and "**" denotes a water sample collected on an unsuccessful core deployment with likely sediment disturbance.

Table A4 Oregon Bulk Sediment (ORBS). REE values for ORBS reported in μg REE per g sediment.

Table A5 Sediment Digest REEs. REE concentrations in sediment digested in a mixture of HNO_3, HCl and HF (procedures of Muratli et al. 2012) from the Oregon slope sites (HH500, HH1200, HH3000) reported in μg REE per g sediment.

Table A6 REE flux by site. a) Fitting parameters for non-linear diffusion calculations at HH1200 and HH3000. M1 is equivalent to the concentration at the depth of the maximum elemental concentration, M2 is the concentration in the bottom water, and M3 is the attenuation coefficient of concentration with depth. The $\chi 2$ and r values for each fit are provided. Fluxes are calculated by equation $y=C_z - (C_z-C_0) \times \exp(\alpha x)$ using both D and Ds. The Ds based flux is also presented as a value normalized to PAAS. **b**) Linear concentration gradients ($\delta C/\delta z$) for each element at all three sites calculated from the depth of maximum concentration to the bottom water. Fluxes are calculated as $F=-D(\delta C/\delta z)$ and $F=-Ds(\delta C/\delta z)$ for each site. Negative flux values represent diffusion from

the pore fluids into the bottom waters. **c**) Estimate of error for the Nd flux from HH3000 based on fitting parameters and error from **(a)**. Porosity and diffusion coefficients remained unchanged. The error introduced by the value of the gradient (C_z-C_0) had the least influence on the overall flux results, and the greatest deviation from the value reported in (**a**) resulted from a maximum error on both α and the gradient.

Table A7 Diffusive Flux Estimates. Nd flux from the pore fluids into the overlying water reported in mol Nd yr^{-1} x 10^6. All fluxes are calculated based on a flux out of the sediments of 31.8 pmol Nd cm^{-2} yr^{-1} and of 13.1 pmol Nd cm^{-2} yr^{-1}. Depth, province, and basin divisions and areas from Menard and Smith (1966). Sediment type coverage areas from Open University (1989) with calculations as described in Appendix A.5.

Table A8 ICP-MS Settings. Characteristics and settings for the ICP-MS used for REE concentration analysis including isotopes monitored and data acquisition settings.

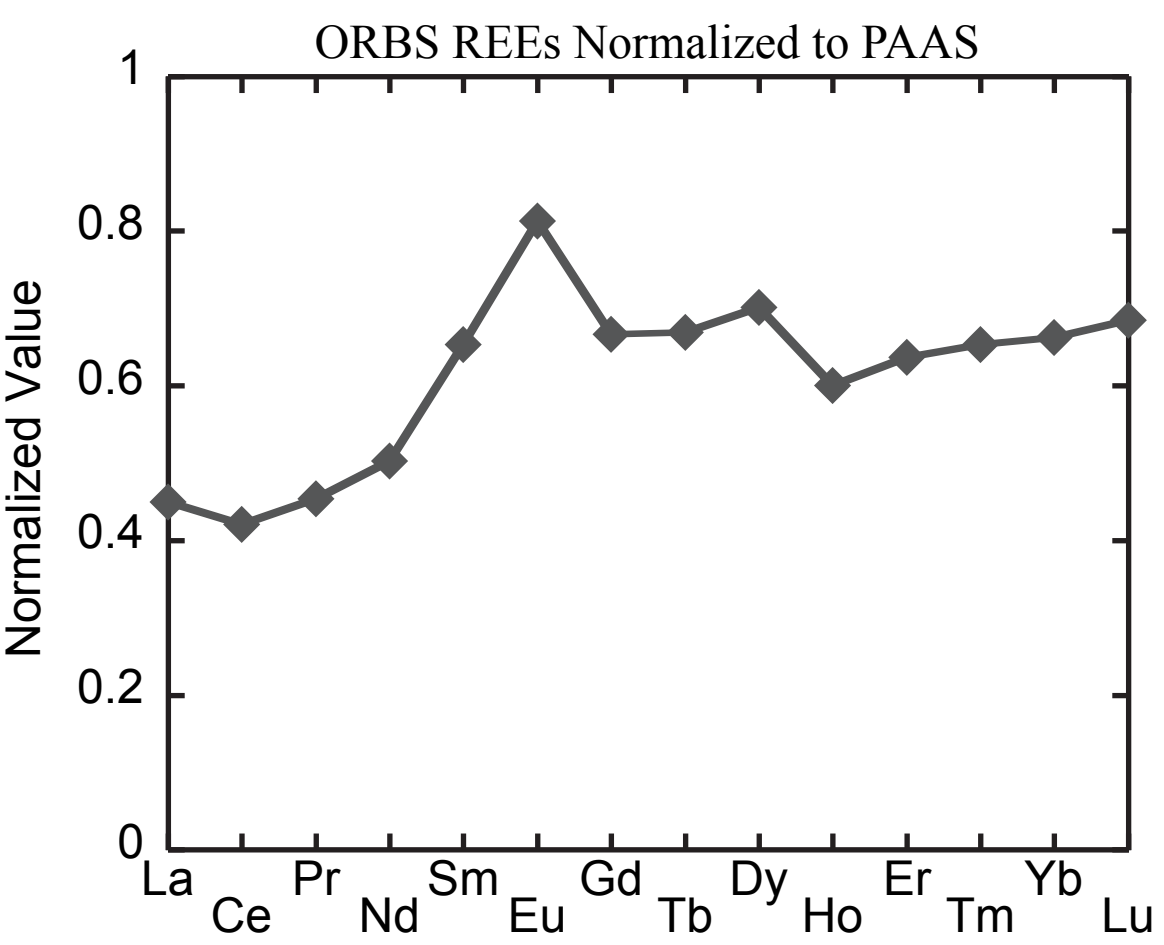
ORBS REEs Normalized to PAAS
Normalized Value
1
0.8
0.6
0.4
0.2
0
La
Ce
Pr
Nd
Sm
Eu
Gd
Tb
Dy
Ho
Er
Tm
Yb
Lu

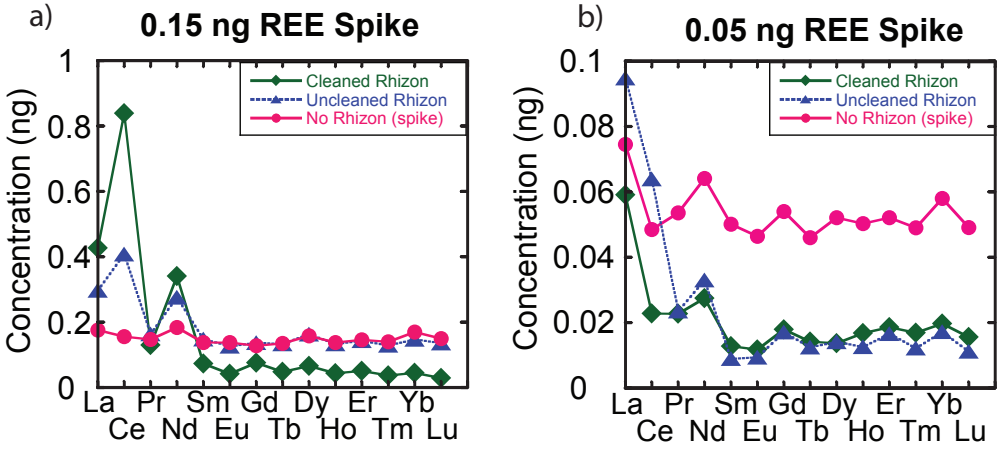
a)
0.15 ng REE Spike
Concentration (ng)
1
0.8
0.6
0.4
0.2
0
Cleaned Rhizon
Uncleaned Rhizon
No Rhizon (spike)
La Ce Pr Nd Sm Eu Gd Tb Dy Ho Er Tm Yb Lu
b)
0.05 ng REE Spike
Concentration (ng)
0.1
0.08
0.06
0.04
0.02
0
Cleaned Rhizon
Uncleaned Rhizon
No Rhizon (spike)
La Ce Pr Nd Sm Eu Gd Tb Dy Ho Er Tm Yb Lu

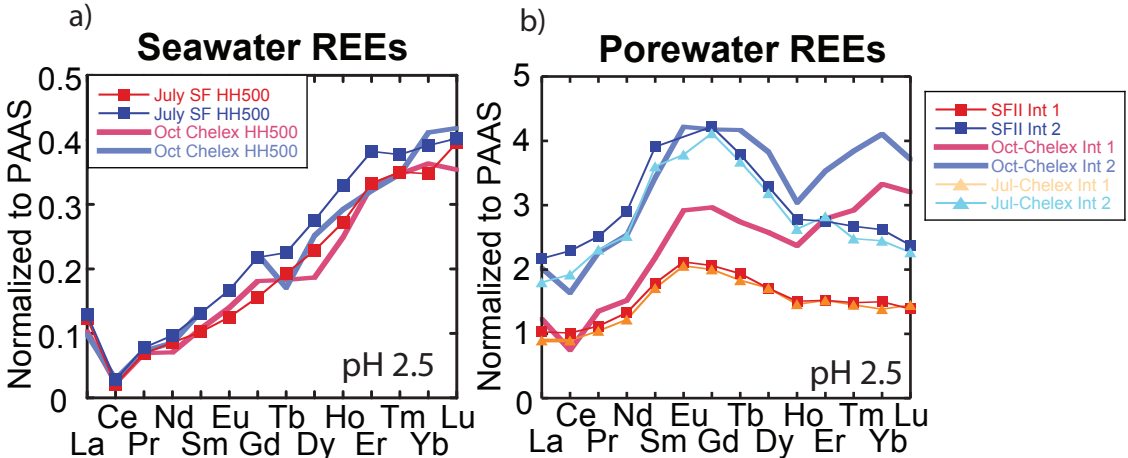
a)
Seawater REEs
Normalized to PAAS
0.5
0.4
0.3
0.2
0.1
0
July SF HH500
July SF HH500
Oct Chelex HH500
Oct Chelex HH500
pH 2.5
La Ce Pr Nd Sm Eu Gd Tb Dy Ho Er Tm Yb Lu
b)
Porewater REEs
Normalized to PAAS
5
4
3
2
1
0
SFII Int 1
SFII Int 2
Oct-Chelex Int 1
Oct-Chelex Int 2
Jul-Chelex Int 1
Jul-Chelex Int 2
pH 2.5
La Ce Pr Nd Sm Eu Gd Tb Dy Ho Er Tm Yb Lu

Station 1

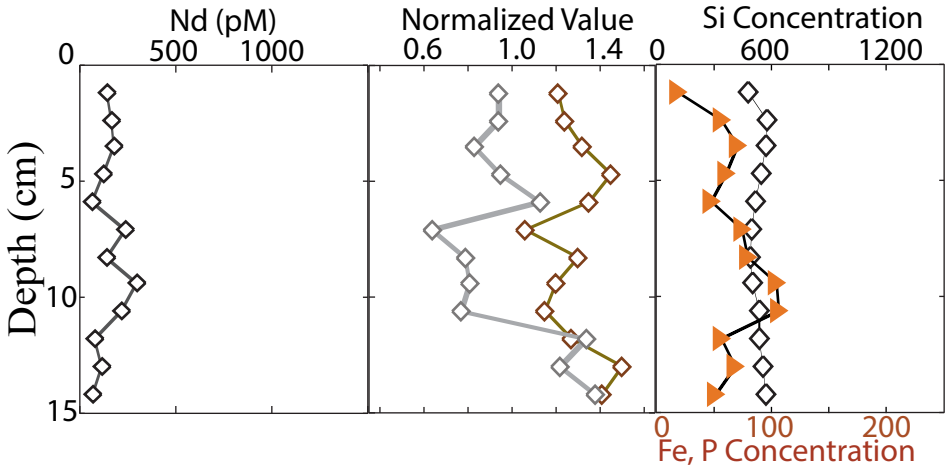

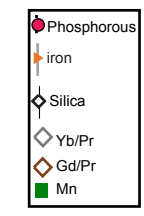

Station 2

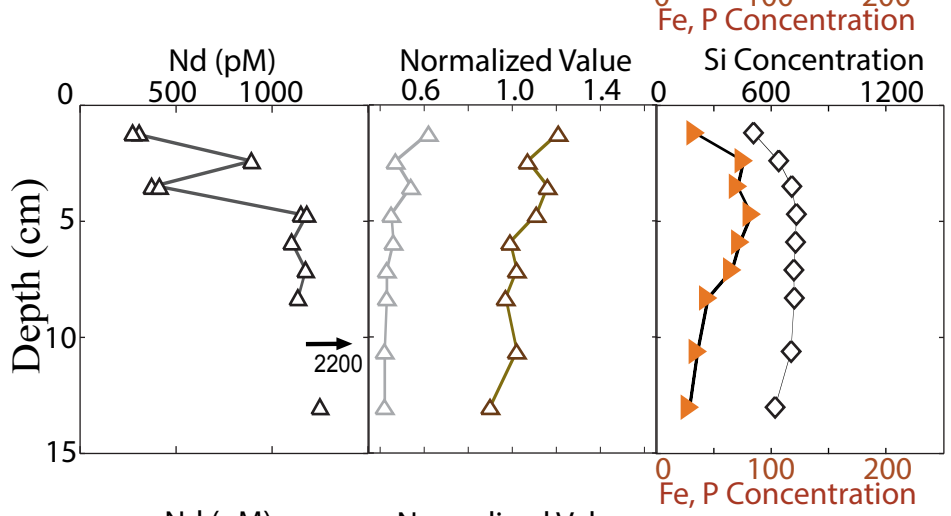

HH200

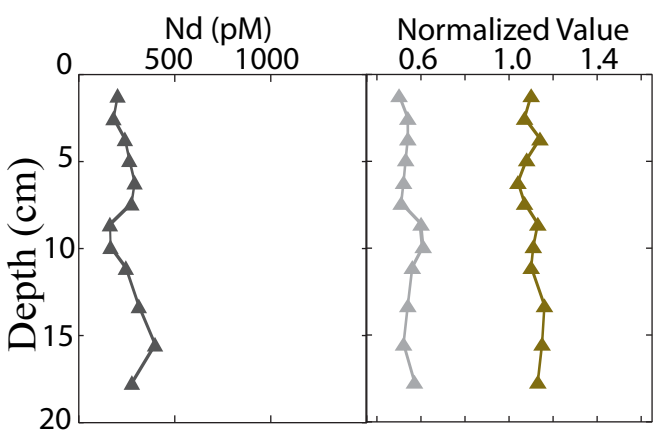

HH500

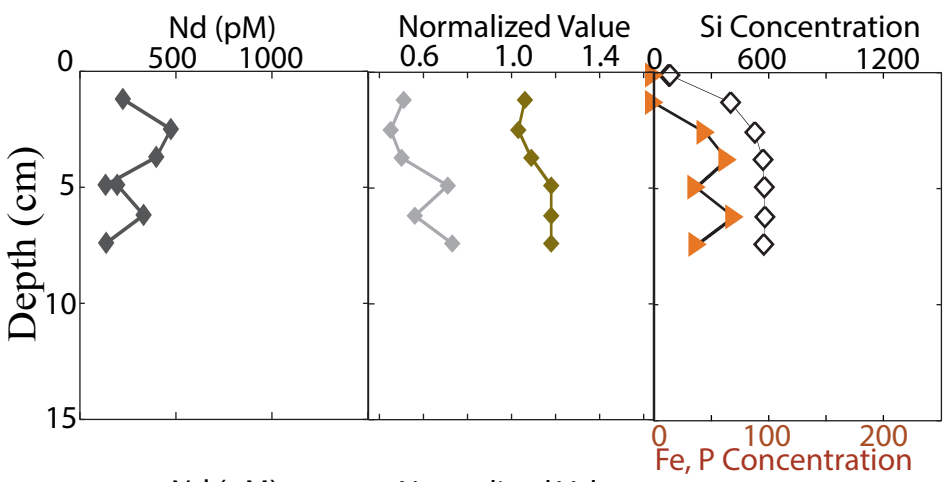

HH1200

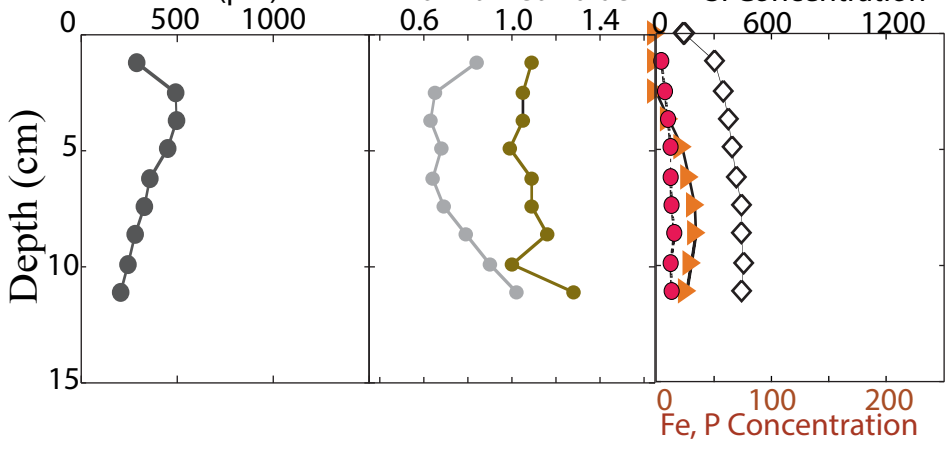

HH3000

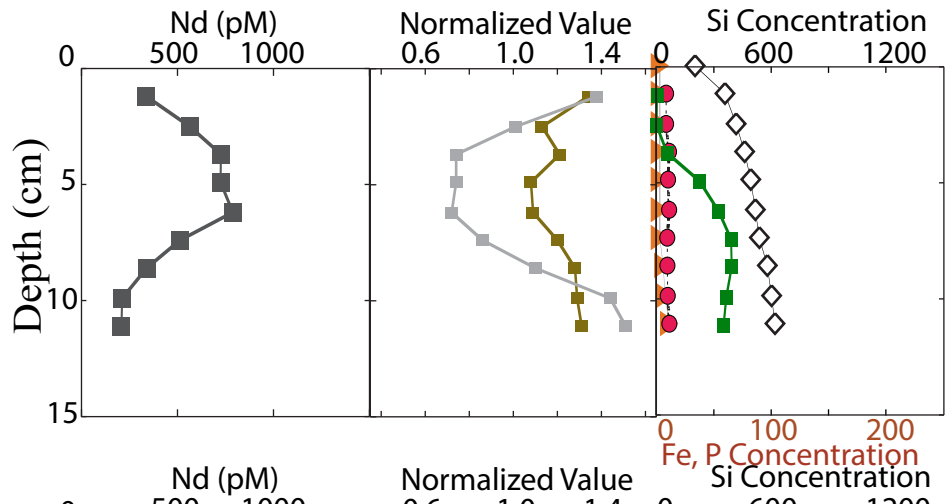

Station 3

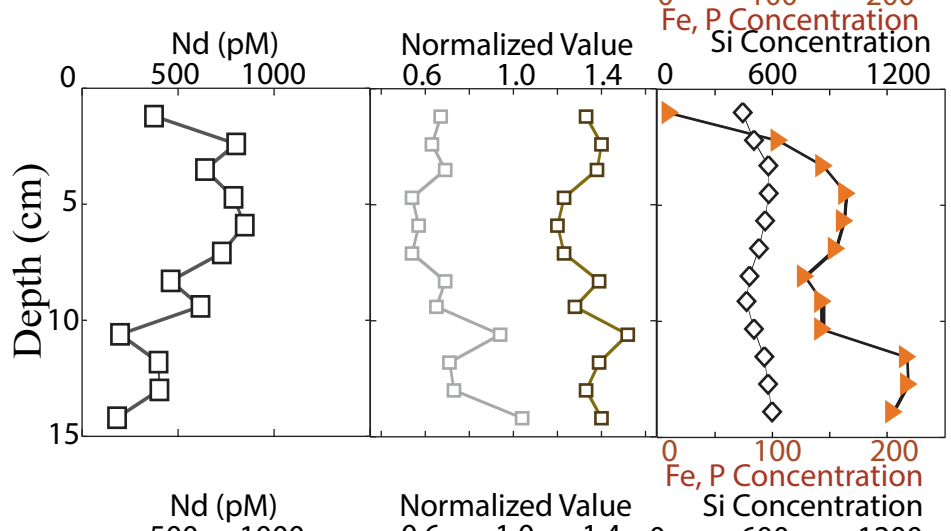

Station 6